EUROPEAN RESPIRATORY *journal*

FLAGSHIP SCIENTIFIC JOURNAL OF ERS

Early View

Original research article

Myeloid cell-specific deletion of inducible nitric oxide synthase protects against smoke-induced pulmonary hypertension in mice

Marija Gredic, Cheng-Yu Wu, Stefan Hadzic, Oleg Pak, Rajkumar Savai, Baktybek Kojonazarov, Siddartha Doswada, Astrid Weiss, Andreas Weigert, Andreas Guenther, Ralf P. Brandes, Ralph T. Schermuly, Friedrich Grimminger, Werner Seeger, Natascha Sommer, Simone Kraut, Norbert Weissmann

Please cite this article as: Gredic M, Wu C-Y, Hadzic S, *et al*. Myeloid cell-specific deletion of inducible nitric oxide synthase protects against smoke-induced pulmonary hypertension in mice. *Eur Respir J* 2021; in press (https://doi.org/10.1183/13993003.01153-2021).

This manuscript has recently been accepted for publication in the *European Respiratory Journal*. It is published here in its accepted form prior to copyediting and typesetting by our production team. After these production processes are complete and the authors have approved the resulting proofs, the article will move to the latest issue of the ERJ online.

Copyright ©The authors 2021. This version is distributed under the terms of the Creative Commons Attribution Non-Commercial Licence 4.0. For commercial reproduction rights and permissions contact permissions@ersnet.org

Myeloid cell-specific deletion of inducible nitric oxide synthase protects against smoke-induced pulmonary hypertension in mice

Marija Gredic[1], Cheng-Yu Wu[1], Stefan Hadzic[1], Oleg Pak[1], Rajkumar Savai[1,2], Baktybek Kojonazarov[1,3], Siddartha Doswada[1], Astrid Weiss[1], Andreas Weigert[4], Andreas Guenther[1,5,6], Ralf P. Brandes[7,8], Ralph T. Schermuly[1], Friedrich Grimminger[1], Werner Seeger[1,2], Natascha Sommer[1], Simone Kraut[1] and Norbert Weissmann[1,*]

[1]Cardio-Pulmonary Institute (CPI), Universities of Giessen and Marburg Lung Center (UGMLC), Member of the German Center for Lung Research (DZL), Justus-Liebig-University, Giessen, Germany

[2]Max Planck Institute for Heart and Lung Research, Member of the German Center for Lung Research (DZL), Bad Nauheim, Germany

[3]Institute for Lung Health (ILH), Justus-Liebig-University, Giessen, Germany

[4]Institute of Biochemistry I, Faculty of Medicine, Goethe-University Frankfurt, Frankfurt, Germany

[5]European IPF Registry & Biobank (eurIPFreg), Giessen, Germany

[6]Agaplesion Evangelisches Krankenhaus Mittelhessen, Giessen, Germany

[7]Institute for Cardiovascular Physiology, Faculty of Medicine, Goethe-University Frankfurt, Germany

[8]DZHK – German Center for Cardiovascular Research, Partner site Rhine-Main

*Correspondence:

Norbert Weissmann, PhD

Universities of Giessen and Marburg Lung Center (UGMLC), Cardio-Pulmonary Institute (CPI)

Aulweg 130, D-35392 Giessen, Germany

Phone +496419942414

Fax +496419942419

e-mail: Norbert.Weissmann@innere.med.uni-giessen.de

Keywords: COPD, pulmonary hypertension, iNOS, macrophages, myeloid cells, pulmonary artery smooth muscle cells.

ABSTRACT

Pulmonary hypertension (PH) is a common complication of chronic obstructive pulmonary disease (COPD), associated with increased mortality and morbidity. Intriguingly, pulmonary vascular alterations have been suggested to drive emphysema development. We previously identified inducible nitric oxide synthase (iNOS) as an essential enzyme for development and reversal of smoke-induced PH and emphysema, and showed that iNOS expression in bone-marrow-derived cells drives pulmonary vascular remodelling, but not parenchymal destruction. In this study, we aimed to identify the iNOS-expressing cell type driving smoke-induced PH and to decipher pro-proliferative pathways involved.

To address this question we used 1) myeloid cell-specific iNOS knockout mice in chronic smoke exposure, 2) co-cultures of macrophages and pulmonary artery smooth muscle cells (PASMC) to decipher underlying signalling pathways.

Myeloid cell-specific iNOS knockout prevented smoke-induced PH but not emphysema in mice. Moreover, iNOS deletion in myeloid cells ameliorated the increase in expression of CD206, a marker of M2 polarization, on interstitial macrophages. Importantly, the observed effects on lung macrophages were hypoxia-independent, as these mice developed hypoxia-induced PH. *In vitro*, smoke-induced PASMC proliferation in co-cultures with M2-polarized macrophages could be abolished by iNOS deletion in phagocytic cells, as well as by ERK inhibition in PASMC. Crucially, CD206-positive and iNOS-positive macrophages accumulated in proximity of remodelled vessels in the lungs of COPD patients, as shown by immunohistochemistry.

In summary, our results demonstrate that iNOS deletion in myeloid cells confers protection against PH in smoke-exposed mice and provide evidence for an iNOS-dependent communication between M2-like macrophages and PASMC in underlying pulmonary vascular remodelling.

INTRODUCTION

Chronic obstructive pulmonary disease (COPD) represents one of the five leading causes of death worldwide. Pathological changes in COPD are caused by inhalation of noxious agents such as cigarette smoke and comprise chronic airway inflammation and progressive alveolar destruction, resulting in chronic bronchitis and emphysema [1, 2]. Underlying molecular mechanisms leading to COPD include increased oxidative stress, the imbalance between proteolytic activity and anti-proteolytic defence and influx of inflammatory cells [3, 4]. Additionally, recent findings from preclinical models [5-8] and COPD patients [9] prompted the hypothesis that pulmonary vascular alterations are an early phenomenon of the COPD pathology and a possible driver of emphysema [10]. In smoke-exposed mice and guinea pigs, pulmonary vascular remodelling precedes parenchymal destruction [5-8] and established therapies for pulmonary hypertension (PH) affect the development of emphysema [11-13]. Moreover, histopathological signs of pulmonary vascular remodelling have been found in most COPD patients and smokers who had not developed COPD [9]. In addition, abnormally high mean pulmonary arterial pressure is present in up to 90% of COPD patients. According to the current WHO classification, COPD-associated pulmonary hypertension (COPD-PH) is included in group 3 of PH (PH due to lung diseases/hypoxia) [14-16]. Although PH is associated with increased risk of exacerbations and decreased survival in COPD patients, efficient pharmacological options are not available [14]. Some of the mechanisms implicated in the pathogenesis of COPD-PH are endothelial dysfunction, hypoxia, vascular pruning and loss of capillary bed [17]. Moreover, activation of inflammatory cells might be contributing to PH development in COPD, as increased systemic levels of several cytokines such as tumour necrosis factor (TNF)-α, C-reactive protein (CRP) [18] and interleukin (IL)-6 [19] were associated with PH in COPD patients and the number of perivascular inflammatory cells correlated with pulmonary vascular alterations [20]. These findings are of even more interest as the prominent role of inflammation in pulmonary vascular remodelling was already recognized in other forms of PH [21-23], although it was previously shown that vascular gene regulation occurring in COPD-PH largely differs from other types of this pulmonary vascular disease [5]. Furthermore, we recently identified inducible nitric oxide synthase (iNOS) as the key player in the pathogenesis of smoke-induced PH as well as emphysema. In smoke-

exposed mice, iNOS inhibition prevented and reversed parenchymal destruction, PH and pulmonary vascular remodelling. Moreover, we demonstrated that iNOS expression in bone-marrow-derived cells is driving the pulmonary vascular alterations, but not emphysema development [5]. However, it remained unclear which bone-marrow-derived cell type drives the process and what the respective mechanism is. We hypothesized here that pathological signalling leading to smoke-induced PH is triggered by elevated iNOS expression in myeloid cells, that macrophages play a critical role, and that a similar process as in the mouse may occur in humans. iNOS is an inducible, calcium-independent and high throughput isoform of nitric oxide synthase, an enzyme generating nitric oxide from L-arginine and molecular oxygen. This enzyme has a prominent role in the immune system, which goes beyond its antimicrobial and antifungal activities and involves effects on the phenotype of the expressing cell, but also on the function and composition of neighbouring immune cells [24].

MATERIALS AND METHODS

Animal model

Adult male and female iNos LysM-Cre mice ($Nos2^{tm2904.1Arte}Tg(CAG\text{-}flpe)2ArteLyz2^{tm1(cre)lfo}$/), 3-4 months old, and age and gender-matched wildtype controls (C57BL/6N, from Charles River Laboratories, Sulzfeld, Germany) were randomly allocated to either tobacco-smoke-exposed or unexposed groups, and to either hypoxic or normoxic groups. All animal experiments were approved by the regional board for animal welfare (Regierungspräsidium Giessen, Germany).

Immunohistochemical staining of human lung sections

Human lung samples from donors and COPD patients were used. The study complied with the Declaration of Helsinki, and the tissue donation protocol was approved by the Ethics Committee of the faculty of medicine at Justus-Liebig University of Giessen, Germany. Immunohistochemical staining was done as previously reported [25] with subtle modifications. Primary antibodies were used as follows: CD68 (Cat#ab955, Abcam, Cambridge, UK; 1:200); CD206 (Cat#ab64693, Abcam, Cambridge, UK; 1:100), anti-iNOS (Cat#NB300-605, Novus Biologicals, Littleton, CO, USA; 1:250), phospho p42/p44 (Cat#4370, Cell Signaling Technology, Danvers, MA, USA; 1:200).

Statistical analysis

Statistical analyses were performed using GraphPad Prism 6 (LaJolla, USA). All data are expressed as means ± standard error of the mean (SEM). Comparison between multiple groups was performed by analysis of variance (two-way ANOVA and Tukey's post-hoc test for comparison between different groups of non-matched samples (animal experiments) and Sidak's post-hoc test for matched samples (cell culture experiments). Independent T-test was used for comparing equality of means between two groups. p-values of <0.05 were considered statistically significant.

Information about all other methods used in this study can be found in the online supplement.

RESULTS

iNOS deletion in myeloid cells prevents PH and right ventricular hypertrophy in smoke-exposed mice

Considering our previous finding that iNOS-expressing, bone-marrow-derived cells drive development of smoke-induced PH, we generated myeloid cell-specific iNOS knockout mice by crossing iNOS$^{flox/flox}$ mice with Lysozyme M promoter-driven Cre expressing mice (hereafter LysM-Cre), to assess the role of myeloid cell-specific iNOS expression in development of smoke-induced PH *in vivo*. Successful generation of the knockout mice was confirmed *in vitro* by quantification of iNOS expression in bone-marrow-derived macrophages (Figure S1a, b), and *in situ*, by immunofluorescent staining of mouse lung sections (Figure S1c).

Hemodynamic measurements following chronic smoke exposure revealed that myeloid cell-specific iNOS knockout mice were protected against PH compared to wildtype (WT) mice when exposed to smoke for 3 and 8 months (Figure 1a). In addition, right ventricular (RV) hypertrophy and impaired RV function occurring after smoke exposure in WT animals were absent in iNOS LysM-Cre mice, as shown by Fulton index and echocardiography (Figures 1b, c). Moreover, muscularization of small pulmonary vessels increased in cigarette smoke-exposed WT mice compared to unexposed (room air) controls after 3 and 8 months (Figure 1d). In contrast, iNOS LysM-Cre mice were fully protected against smoke-induced pulmonary vascular remodelling.

Myeloid cell-specific iNOS knockout does not prevent emphysema development in mice after chronic smoke exposure

In parallel, we investigated the development of emphysema in iNOS LysM-Cre mice. We first used fluorescent molecular tomography combined with micro-computed tomography (FMT-μCT) and Annexin V-based imaging probe to quantify apoptosis *in vivo* and found an increase in apoptosis in lungs of both WT and iNOS LysM-Cre mice after 8 months of smoke exposure, compared to respective unexposed (room air) controls (Figure 2a). Functional measurements with the FlexiVent system (Figure 2b), assessment of functional residual capacity by μCT (Figure 2c), and morphometric analysis including design-based stereology (Figure 2d and S2) confirmed emphysema development in both WT and iNOS LysM-Cre mice after 8 months of chronic smoke exposure. Baseline values and temporal dynamic of lung function changes were different in knockout animals, possibly due to congenital effects.

iNOS deletion in myeloid cells affects composition of inflammatory cells in lungs after chronic smoke exposure

As the composition and phenotype of lung inflammatory cells are important factors in other forms of PH, we next examined the effects of myeloid-cell specific iNOS deletion on smoke-induced changes in immune cells in lung homogenate using flow cytometry. After 8 months of chronic smoke exposure, a significant increase in the portion of interstitial macrophages (characterized as shown in Figure 3a) in $CD45^+$ cells was found in lung homogenates of smoke-exposed WT animals compared to respective unexposed (room air) controls, but was absent in iNOS LysM-Cre mice (Figure 3b). Considering the finding that the shift towards an M2-like phenotype of macrophages contributes to pulmonary vascular remodelling in other forms of PH, we next examined the expression of CD206 on interstitial macrophages found in the lung homogenate after chronic smoke exposure. This analysis revealed in WT animals a significant increase in the expression of CD206, suggesting a smoke-induced shift of interstitial macrophages towards an M2-like phenotype. Importantly, CD206 expression on interstitial macrophages in lungs of iNOS LysM-Cre mice remained unchanged (Figures 3c, d).

Additionally, we found that the smoke-induced increase in the proportion of $CD4^+$ T-cells in $CD45^+$ cells in lung homogenate was significantly higher in WT compared to iNOS LysM-Cre animals. Similarly, there was a tendency towards a higher smoke-induced increase in both $CD4^+$ and $CD8^+$ T-cells in broncho-alveolar lavage (BAL) of WT compared to iNOS LysM-Cre mice (Figure S3a, b).

iNOS deletion in myeloid cells does not affect development of hypoxia-induced PH and right ventricular hypertrophy

As alveolar hypoxia caused by impairment of respiratory function can contribute to vascular remodelling in COPD [17], and the M2 phenotype of macrophages is important for development of hypoxia-induced PH [26], we investigated whether iNOS deletion in myeloid cells can also protect mice against PH after exposure to chronic hypoxia. However, myeloid cell-specific iNOS knockout mice developed hypoxia-induced PH to the same level as observed in WT mice. This was evident from hemodynamic measurements (Figure 4a), determination of RV hypertrophy, and the decrease of RV function (Figure 4b, c). Chronic hypoxia led to a similar increase in the degree of muscularization of small pulmonary vessels in both genotypes (Figure 4d).

Cigarette smoke extract (CSE) treatment of M2 macrophages increases proliferation and migration of co-cultured PASMC in an iNOS-dependent manner

Based on the prominent iNOS-dependent changes in the portion and phenotype of interstitial macrophages in lungs upon smoke exposure, we next investigated the proliferation of murine primary PASMC co-cultured with bone-marrow-derived and CSE-stimulated macrophages by the use of a Transwell system (Figure 5a). For the treatment, we chose a concentration of CSE that did not affect viability/metabolic activity of macrophages even during prolonged exposure (Figure S4a). Pre-treatment of M2, but not of M1 or naïve macrophages with CSE increased proliferation of PASMC in co-culture after 6h and 24h (Figure 5a). Intriguingly, deletion of iNOS in M2 macrophages abolished the CSE-dependent increase of PASMC proliferation (Figure 5a). In addition, this effect was dependent on the communication between the co-cultured cell types, because it was absent when PASMC were not co-cultured but were treated with macrophage culture-conditioned medium (CM, Figure S4b).

Moreover, we examined the effects of the crosstalk between macrophages and PASMC on migration and apoptosis of PASMC by treatment of PASMC in monoculture with co-culture CM. As in the case of proliferation of co-cultured (Figure 5a) or co-culture CM-treated PASMC, the pro-migratory effect of co-culture CM on PASMC was increased by CSE treatment of M2 macrophages and abolished by iNOS inhibition in these cells (Figure S5a). However, CM from co-cultures decreased PASMC apoptosis and that effect was not dependent on CSE-treatment of M2 macrophages nor iNOS activity in these cells (Figure S5b).

IL-4 and MAPK signalling might contribute to CSE-induced iNOS-dependent proliferation of PASMC in co-cultures

Next, we examined the mechanism by which M2 macrophages in co-culture trigger the proliferation of PASMC. These investigations revealed an increase in phosphorylation of extracellular signal-regulated kinase (ERK) in PASMC at early time-points (1h, 3h and 6h) after co-culturing. Such an increase of phospho-ERK was absent upon L-NIL treatment of the phagocytic cells (Figure 5b and S6a). The fact that the pattern of ERK phosphorylation resembled PASMC proliferation suggested a functional role of ERK phosphorylation in the CSE-M2-macrophage driven proliferation. To prove this suggestion we investigated whether ERK inhibition affected PASMC proliferation when treated with co-culture CM. Indeed, the ERK1/2 inhibitor SCH772984 inhibited the increase in PASMC proliferation induced by CM from PASMC-M2 (CSE-pre-treated) macrophage co-cultures (Figure 5c and S6c). This effect was similar to the effect of iNOS inhibition (Figure 5c). Crucially, these results are consistent with our *in vivo* data, where smoke exposure increases ERK1/2 phosphorylation in pulmonary vessels (Figure 5d) and in lung homogenates (Figure S6c) of WT but not of knockout animals.

Additionally, cytokine profiling in the co-culture medium revealed decreased concentrations of IL-4 in co-cultures of PASMC with M2 macrophages when treated with L-NIL (Figures 6a, b). Functionally, the application of recombinant IL-4 in co-cultures of PASMC with M2 macrophages reversed the reduction of CSE-induced proliferation caused by L-NIL-treatment of M2 macrophages (Figure 6c).

iNOS$^+$ and CD206$^+$ macrophages accumulate in close proximity of remodelled vessels in lungs of COPD patients

To investigate the relevance of the described findings for human COPD, we performed double staining of human lung sections for the macrophage marker CD68 and iNOS and found an increased number of iNOS-expressing macrophages in the proximity of the remodelled vessels in COPD patients when compared to donors (Figure 7a). Additionally, we stained human COPD lungs for CD68 and CD206, a protein highly expressed by alternatively activated M2-like macrophages, and found numerous double-positive cells around the remodelled vessels in COPD lungs (Figure 7b). Similar to our findings in mouse lungs, immunohistochemical staining localized a high expression of phosphorylated ERK1/2 in the vessel media of COPD lungs compared to healthy donor controls (Figure 7c). Increase in ERK1/2 phosphorylation in lungs of COPD patients compared to healthy donors was also confirmed by Western blot analysis (Figure 7d). These data thus support our conclusion of an important role of M2 macrophages for pulmonary vascular remodelling.

DISCUSSION

Our study revealed that myeloid cell-specific deletion of iNOS 1) prevents the development of smoke-induced PH, but not emphysema, 2) in contrast does not prevent hypoxia-induced PH, 3) counteracts the increase in expression of the marker of M2 polarization (CD206) on interstitial macrophages in smoke-exposed lungs. Moreover, we provided evidence for 4) the iNOS-dependent crosstalk between M2-polarized macrophages and PASMC that drives proliferation of PASMC in cigarette smoke-induced PH, and 5) the involvement of phospho-ERK and IL-4 in the downstream signalling processes (Figure 8). Similar recruitment of M2-like, iNOS containing macrophages as in our mouse model occurred in human COPD lungs in close proximity to pulmonary vessels.

Since pulmonary vascular remodelling is an early hallmark of COPD pathology [9], it was hypothesized that this remodelling can contribute to or even drive emphysema development. However, the existence of emphysema in myeloid cell-specific iNOS knockout animals upon smoke exposure supports our previous finding that PH and parenchymal destruction can occur

independently [5]. Nevertheless, there is a possibility that molecular alterations in the vasculature (and not remodelling *per se*) are driving parenchymal destruction. Such a situation would explain emphysema development in the absence of pulmonary vascular remodelling but (co)driven by vascular molecular alterations, as iNOS upregulation primarily in the vascular compartment of the lungs leads to parenchymal destruction [5].

Although the pivotal role of inflammatory cells and their mediators in other forms of PH is well substantiated by experimental evidence in rodent models and patients [21-23], only a few studies, mentioned in the introduction, have addressed the role of inflammation in COPD-PH. Our study, however, to the best of our knowledge, is the first to implicate macrophages as the inflammatory cell-type driving smoke-induced PASMC proliferation and consequent pulmonary vascular remodelling in an iNOS dependent manner. We used a driver line targeting all myeloid cells, which by its specificity goes beyond previous studies from bone-marrow transplantation experiments and rules out shortcomings of these previous experimental approaches such as the effects of radiation and reconstitution [5, 27-29]. Our experiments revealed that macrophages seem the most important candidates of the myeloid cell lineage, because 1) iNOS plays an important role in these cells [30, 31], 2) of their presence in pulmonary vessels upon smoke exposure, and 3) of their effect on PASMC proliferation in our *in vitro* experiments. Intriguingly, we demonstrated that there is a cross-talk between macrophages and PASMC, which drives proliferation of those vascular cells and can be prevented by inhibiting or deleting M2 macrophage-derived iNOS. In agreement with our findings, a recent study reported a two-way communication between M2 macrophages and PASMC, which relies on both CCR2 and CCR5 and drives proliferation of PASMC *in vitro* and pulmonary vascular remodelling in IPAH and animal hypoxia and SU5416/hypoxia models of PH *in vivo* [22]. However, no data exist for group 3 PH [16], neither has the role of iNOS in these cells been addressed in the context of group 3 PH. Although our data support the concept that M2 macrophage-derived signals are important contributors to pulmonary vascular remodelling, we could not find smoke- or iNOS-dependent changes in the levels of CCR2 and CCR5 (unpublished observations), suggesting that there is indeed a unique molecular signature of the vasculature in COPD-PH, as previously suggested by our laboratory [5]. This conclusion is supported by our finding that iNOS deletion in myeloid cells

protects against smoke-induced, but not hypoxia-induced PH (for a detailed discussion please refer to the online supplementary material).

There are two important effects of myeloid cell-specific iNOS deletion on the composition and the phenotype of lung inflammatory cells upon smoke exposure, which may amplify *in vivo* the anti-proliferative effect of iNOS inhibition in M2 cells observed in our co-culture system.

First, the smoke-induced increase in the expression of CD206 on interstitial macrophages was not observed in our knockout mice, suggesting protection against the smoke-induced shift towards the M2-like phenotype. This is of even more interest, as iNOS is considered to be a classical marker of M1 polarization. However, recent and partially contradicting reports suggest that this pleiotropic enzyme can influence polarization of expressing macrophages. Van den Bossche and colleagues reported that iNOS expression prevented repolarization of macrophages from M1 to M2 phenotype, presumably through the inhibitory effect on oxidative phosphorylation [32]. Conversely, Lu and colleagues recently showed that myeloid cell-derived iNOS suppressed M1 macrophage polarization and speculated that it supports dedifferentiation and phenotypic plasticity of these cells, without affecting the M2 macrophage population [33]. Although the concept that iNOS is a regulator of gene expression and phenotype of macrophages can be easily applied to our findings, none of the described scenarios can completely explain protection of myeloid cell-specific iNOS knockout against smoke-induced PH or differential smoke-induced effects of WT and iNOS-deficient M2 macrophages on PASMC proliferation in co-culture. Due to the dynamic nature of macrophage phenotypes, it is likely that micro-environmental factors such as smoke and signals from PASMC *in vitro*, and additionally the age of animals, apoptosis of lung epithelial cells and presence of other inflammatory cell types and mediators *in vivo* contribute to the specific behaviour of macrophages observed in our models upon smoke exposure.

The second important consequence of myeloid cell-specific iNOS deletion on the composition of inflammatory cell infiltrates is the preserved proportion of T-cells in the population of lung immune cells (discussed in more detail in supplementary material).

Regarding the potential molecular mechanisms, our results indicate a regulatory role of iNOS in macrophage polarization, in the response of M2 macrophages to smoke and in the pro-

proliferative communication between PASMC and M2 macrophages. Since such effects were not observed for M1 cells, mechanistically they are probably not caused by the production of large amounts of nitric oxide and consequent nitrosative stress, but rather by protein nitration as a regulatory posttranslational modification. Such a situation was observed before for the regulation of Janus tyrosine kinase (TYK)-2 downstream of IL-12 receptor and retinoic acid receptor-related orphan receptor (ROR)-γT, in the processes of functional maturation of NK and T-cells, respectively [34, 35]. The specificity of the iNOS-dependent regulation observed in our smoke-challenged M2 macrophages is further supported by the finding that deletion of this enzyme abolished their smoke-induced proliferative and pro-migratory signalling to PASMC in co-culture, but did not influence anti-apoptotic effects that conditioned medium from such co-cultures exerted on PASMC. Intriguingly, judging from our *in vitro* experiments, the regulatory role of iNOS in pro-proliferative signalling of M2 cells is unique for specific conditions, which include both exposure of macrophages to smoke and communication between macrophages and PASMC. Importantly, immunohistochemical staining of human lungs suggests that similar conditions exist in COPD, as the macrophages that accumulated in close vicinity to remodelled vessels in the lungs of COPD patients were positive for iNOS and CD206.

Focussing on the iNOS-dependent signalling events, our experiments revealed that ERK signalling was upregulated in PASMC co-cultured with M2 macrophages and in lungs of smoke-exposed WT animals. Functionally, inhibition of this pathway in PASMC successfully counteracted pro-proliferative signals from M2 macrophages in our co-culture model. We demonstrated the relevance for human COPD, as our immunohistochemical analysis for phosphorylated ERK revealed a prominent upregulation, located in the remodelled vessels in the lungs of COPD patients. Although activation of this pathway in COPD lungs was previously investigated in the context of other anatomic lesions [36, 37], to the best of our knowledge our study is the first to provide evidence for the involvement of the ERK pathway in remodelling of the pulmonary vessel media in human COPD. Taken together, these results demonstrate that ERK signalling, implicated in other forms of PH [38-40], might also be important for smoke-induced vascular remodelling and is driven by iNOS. Furthermore, our results suggest that activation of the ERK pathway and

consequent PASMC proliferation is an early event after the contact with smoke-challenged M2 macrophages.

In addition, our findings suggest IL-4 as the factor that controls the responsiveness of M2 macrophages to CSE stimulation and thus regulates their pro-proliferative signalling to PASMC. Along these lines, Kumar and colleagues recently demonstrated that IL-4, acting in concert with IL-13, plays a key pathogenic role in transforming growth factor (TGF)-β-mediated, *Schistosoma mansoni*-induced pulmonary arterial hypertension [41]. In accordance with our findings (data not given), the authors did not find increased levels of total TGF-β; instead, they propose that M2 macrophages receiving IL-4/IL-13 signals activate a latent form of this growth factor via a mechanism that has yet to be elucidated. Interestingly, TGF-β is known to induce vascular smooth muscle cell proliferation through activation of the ERK pathway [42, 43]. The connection between iNOS and IL-4, however, needs further investigation. As iNOS is known to promote glycolysis [32, 44] and lactate stimulates IL-4 and IL-13 production [45], it is conceivable that metabolic changes are the missing link connecting these two important players in CSE-induced PASMC proliferation.

CONCLUSIONS

Our data demonstrate that iNOS deletion in myeloid cells protects mice against smoke-induced PH, that M2 macrophages are the most likely candidates of the myeloid cell line driving pulmonary vascular remodelling upon smoke exposure and that crosstalk between M2 macrophages and PASMC is an essential process in this regard. iNOS dependent ERK- and IL-4-signalling have been identified as mechanistic downstream signalling (Figure 8). Similar processes as in our mouse model occur in human COPD. Our data further support the concept that pulmonary vascular remodelling and emphysema can occur independently, but does not rule out that parenchymal destruction can be driven by molecular alterations in vascular cell types.

ACKNOWLEDGEMENTS

The authors thank Karin Quanz, Ewa Bieniek, Ingrid Breitenborn-Müller, Nils Schupp, Carmen Homberger, Susanne Lich, Miriam Wessendorf and Elisabeth Kappes for technical assistance.

FOOTNOTES

- This article has supplementary material available from err.ersjournals.com
- Conflict of interest: None
- Support statement: This work was funded by the Deutsche Forschungsgemeinschaft (DFG, German Research Foundation)–Projektnummer 268555672 – SFB 1213, A07 to N.W. and CP02 to B.K.

LITERATURE

1. Viegi, G., F. Pistelli, D.L. Sherrill, S. Maio, S. Baldacci, and L. Carrozzi, *Definition, epidemiology and natural history of COPD.* Eur Respir J, 2007. **30**(5): p. 993-1013.
2. Barnes, P.J., P.G. Burney, E.K. Silverman, B.R. Celli, J. Vestbo, J.A. Wedzicha, and E.F. Wouters, *Chronic obstructive pulmonary disease.* Nat Rev Dis Primers, 2015. **1**: p. 15076.
3. Barnes, P.J., S.D. Shapiro, and R.A. Pauwels, *Chronic obstructive pulmonary disease: molecular and cellular mechanisms.* Eur Respir J, 2003. **22**(4): p. 672-88.
4. Hadzic, S., C.Y. Wu, S. Avdeev, N. Weissmann, R.T. Schermuly, and D. Kosanovic, *Lung epithelium damage in COPD - An unstoppable pathological event?* Cell Signal, 2020. **68**: p. 109540.
5. Seimetz, M., N. Parajuli, A. Pichl, F. Veit, G. Kwapiszewska, F.C. Weisel, K. Milger, B. Egemnazarov, A. Turowska, B. Fuchs, S. Nikam, M. Roth, A. Sydykov, T. Medebach, W. Klepetko, P. Jaksch, R. Dumitrascu, H. Garn, R. Voswinckel, S. Kostin, W. Seeger, R.T. Schermuly, F. Grimminger, H.A. Ghofrani, and N. Weissmann, *Inducible NOS inhibition reverses tobacco-smoke-induced emphysema and pulmonary hypertension in mice.* Cell, 2011. **147**(2): p. 293-305.
6. Ferrer, E., V.I. Peinado, M. Diez, J.L. Carrasco, M.M. Musri, A. Martinez, R. Rodriguez-Roisin, and J.A. Barbera, *Effects of cigarette smoke on endothelial function of pulmonary arteries in the guinea pig.* Respir Res, 2009. **10**: p. 76.
7. Wright, J.L. and A. Churg, *Effect of long-term cigarette smoke exposure on pulmonary vascular structure and function in the guinea pig.* Exp Lung Res, 1991. **17**(6): p. 997-1009.
8. Seimetz, M., N. Sommer, M. Bednorz, O. Pak, C. Veith, S. Hadzic, M. Gredic, N. Parajuli, B. Kojonazarov, S. Kraut, J. Wilhelm, F. Knoepp, I. Henneke, A. Pichl, Z.I. Kanbagli, S. Scheibe, A. Fysikopoulos, C.Y. Wu, W. Klepetko, P. Jaksch, C. Eichstaedt, E. Grunig, K. Hinderhofer, M. Geiszt, N. Muller, F. Rezende, G. Buchmann, I. Wittig, M. Hecker, A. Hecker, W. Padberg, P. Dorfmuller, S. Gattenlohner, C.F. Vogelmeier, A. Gunther, S. Karnati, E. Baumgart-Vogt, R.T. Schermuly, H.A. Ghofrani, W. Seeger, K. Schroder, F. Grimminger, R.P. Brandes, and N. Weissmann, *NADPH oxidase subunit NOXO1 is a target for emphysema treatment in COPD.* Nat Metab, 2020. **2**(6): p. 532-546.
9. Santos, S., V.I. Peinado, J. Ramirez, T. Melgosa, J. Roca, R. Rodriguez-Roisin, and J.A. Barbera, *Characterization of pulmonary vascular remodelling in smokers and patients with mild COPD.* Eur Respir J, 2002. **19**(4): p. 632-8.
10. Gredic, M., I. Blanco, G. Kovacs, Z. Helyes, P. Ferdinandy, H. Olschewski, J.A. Barbera, and N. Weissmann, *Pulmonary hypertension in chronic obstructive pulmonary disease.* Br J Pharmacol, 2020.
11. Pichl, A., N. Sommer, M. Bednorz, M. Seimetz, S. Hadzic, S. Kuhnert, S. Kraut, E.T. Roxlau, B. Kojonazarov, J. Wilhelm, M. Gredic, H. Gall, K. Tello, M.J. Richter, O. Pak, A. Petrovic, M. Hecker, R.T. Schermuly, F. Grimminger, W. Seeger, H.A. Ghofrani, and N. Weissmann, *Riociguat for treatment of pulmonary hypertension in COPD: a translational study.* Eur Respir J, 2019. **53**(6).
12. Weissmann, N., B. Lobo, A. Pichl, N. Parajuli, M. Seimetz, R. Puig-Pey, E. Ferrer, V.I. Peinado, D. Dominguez-Fandos, A. Fysikopoulos, J.P. Stasch, H.A. Ghofrani, N. Coll-Bonfill, R. Frey, R.T. Schermuly, J. Garcia-Lucio, I. Blanco, M. Bednorz, O. Tura-Ceide, E. Tadele,

R.P. Brandes, J. Grimminger, W. Klepetko, P. Jaksch, R. Rodriguez-Roisin, W. Seeger, F. Grimminger, and J.A. Barbera, *Stimulation of soluble guanylate cyclase prevents cigarette smoke-induced pulmonary hypertension and emphysema.* Am J Respir Crit Care Med, 2014. **189**(11): p. 1359-73.

13. Seimetz, M., N. Parajuli, A. Pichl, M. Bednorz, H.A. Ghofrani, R.T. Schermuly, W. Seeger, F. Grimminger, and N. Weissmann, *Cigarette Smoke-Induced Emphysema and Pulmonary Hypertension Can Be Prevented by Phosphodiesterase 4 and 5 Inhibition in Mice.* PLoS One, 2015. **10**(6): p. e0129327.
14. Nathan, S.D., J.A. Barbera, S.P. Gaine, S. Harari, F.J. Martinez, H. Olschewski, K.M. Olsson, A.J. Peacock, J. Pepke-Zaba, S. Provencher, N. Weissmann, and W. Seeger, *Pulmonary hypertension in chronic lung disease and hypoxia.* Eur Respir J, 2019. **53**(1).
15. Minai, O.A., A. Chaouat, and S. Adnot, *Pulmonary hypertension in COPD: epidemiology, significance, and management: pulmonary vascular disease: the global perspective.* Chest, 2010. **137**(6 Suppl): p. 39S-51S.
16. Simonneau, G., D. Montani, D.S. Celermajer, C.P. Denton, M.A. Gatzoulis, M. Krowka, P.G. Williams, and R. Souza, *Haemodynamic definitions and updated clinical classification of pulmonary hypertension.* Eur Respir J, 2019. **53**(1).
17. Chaouat, A., R. Naeije, and E. Weitzenblum, *Pulmonary hypertension in COPD.* Eur Respir J, 2008. **32**(5): p. 1371-85.
18. Joppa, P., D. Petrasova, B. Stancak, and R. Tkacova, *Systemic inflammation in patients with COPD and pulmonary hypertension.* Chest, 2006. **130**(2): p. 326-33.
19. Eddahibi, S., A. Chaouat, L. Tu, C. Chouaid, E. Weitzenblum, B. Housset, B. Maitre, and S. Adnot, *Interleukin-6 gene polymorphism confers susceptibility to pulmonary hypertension in chronic obstructive pulmonary disease.* Proc Am Thorac Soc, 2006. **3**(6): p. 475-476.
20. Peinado, V.I., J.A. Barbera, P. Abate, J. Ramirez, J. Roca, S. Santos, and R. Rodriguez-Roisin, *Inflammatory reaction in pulmonary muscular arteries of patients with mild chronic obstructive pulmonary disease.* Am J Respir Crit Care Med, 1999. **159**(5 Pt 1): p. 1605-11.
21. Savai, R., S.S. Pullamsetti, J. Kolbe, E. Bieniek, R. Voswinckel, L. Fink, A. Scheed, C. Ritter, B.K. Dahal, A. Vater, S. Klussmann, H.A. Ghofrani, N. Weissmann, W. Klepetko, G.A. Banat, W. Seeger, F. Grimminger, and R.T. Schermuly, *Immune and inflammatory cell involvement in the pathology of idiopathic pulmonary arterial hypertension.* Am J Respir Crit Care Med, 2012. **186**(9): p. 897-908.
22. Abid, S., E. Marcos, A. Parpaleix, V. Amsellem, M. Breau, A. Houssaini, N. Vienney, M. Lefevre, G. Derumeaux, S. Evans, C. Hubeau, M. Delcroix, R. Quarck, S. Adnot, and L. Lipskaia, *CCR2/CCR5-Mediated Macrophage-Smooth Muscle Cell Crosstalk in Pulmonary Hypertension.* Eur Respir J, 2019.
23. Amsellem, V., S. Abid, L. Poupel, A. Parpaleix, M. Rodero, G. Gary-Bobo, M. Latiri, J.L. Dubois-Rande, L. Lipskaia, C. Combadiere, and S. Adnot, *Roles for the CX3CL1/CX3CR1 and CCL2/CCR2 Chemokine Systems in Hypoxic Pulmonary Hypertension.* Am J Respir Cell Mol Biol, 2017. **56**(5): p. 597-608.
24. Bogdan, C., *Nitric oxide synthase in innate and adaptive immunity: an update.* Trends Immunol, 2015. **36**(3): p. 161-78.
25. Kosanovic, D., B.K. Dahal, D.M. Peters, M. Seimetz, M. Wygrecka, K. Hoffmann, J. Antel, I. Reiss, H.A. Ghofrani, N. Weissmann, F. Grimminger, W. Seeger, and R.T. Schermuly,

Histological characterization of mast cell chymase in patients with pulmonary hypertension and chronic obstructive pulmonary disease. Pulm Circ, 2014. **4**(1): p. 128-36.
26. Vergadi, E., M.S. Chang, C. Lee, O.D. Liang, X. Liu, A. Fernandez-Gonzalez, S.A. Mitsialis, and S. Kourembanas, *Early macrophage recruitment and alternative activation are critical for the later development of hypoxia-induced pulmonary hypertension.* Circulation, 2011. **123**(18): p. 1986-95.
27. Kierdorf, K., N. Katzmarski, C.A. Haas, and M. Prinz, *Bone marrow cell recruitment to the brain in the absence of irradiation or parabiosis bias.* PLoS One, 2013. **8**(3): p. e58544.
28. Ajami, B., J.L. Bennett, C. Krieger, W. Tetzlaff, and F.M. Rossi, *Local self-renewal can sustain CNS microglia maintenance and function throughout adult life.* Nat Neurosci, 2007. **10**(12): p. 1538-43.
29. Ferreira, F.M., P. Palle, J. Vom Berg, P. Prajwal, J.D. Laman, and T. Buch, *Bone marrow chimeras-a vital tool in basic and translational research.* J Mol Med (Berl), 2019. **97**(7): p. 889-896.
30. Forstermann, U. and W.C. Sessa, *Nitric oxide synthases: regulation and function.* Eur Heart J, 2012. **33**(7): p. 829-37, 837a-837d.
31. Nathan, C.F. and J.B. Hibbs, Jr., *Role of nitric oxide synthesis in macrophage antimicrobial activity.* Curr Opin Immunol, 1991. **3**(1): p. 65-70.
32. Van den Bossche, J., J. Baardman, N.A. Otto, S. van der Velden, A.E. Neele, S.M. van den Berg, R. Luque-Martin, H.J. Chen, M.C. Boshuizen, M. Ahmed, M.A. Hoeksema, A.F. de Vos, and M.P. de Winther, *Mitochondrial Dysfunction Prevents Repolarization of Inflammatory Macrophages.* Cell Rep, 2016. **17**(3): p. 684-696.
33. Lu, G., R. Zhang, S. Geng, L. Peng, P. Jayaraman, C. Chen, F. Xu, J. Yang, Q. Li, H. Zheng, K. Shen, J. Wang, X. Liu, W. Wang, Z. Zheng, C.F. Qi, C. Si, J.C. He, K. Liu, S.A. Lira, A.G. Sikora, L. Li, and H. Xiong, *Myeloid cell-derived inducible nitric oxide synthase suppresses M1 macrophage polarization.* Nat Commun, 2015. **6**: p. 6676.
34. Jianjun, Y., R. Zhang, G. Lu, Y. Shen, L. Peng, C. Zhu, M. Cui, W. Wang, P. Arnaboldi, M. Tang, M. Gupta, C.F. Qi, P. Jayaraman, H. Zhu, B. Jiang, S.H. Chen, J.C. He, A.T. Ting, M.M. Zhou, V.K. Kuchroo, H.C. Morse, 3rd, K. Ozato, A.G. Sikora, and H. Xiong, *T cell-derived inducible nitric oxide synthase switches off Th17 cell differentiation.* J Exp Med, 2013. **210**(7): p. 1447-62.
35. Diefenbach, A., H. Schindler, M. Rollinghoff, W.M. Yokoyama, and C. Bogdan, *Requirement for type 2 NO synthase for IL-12 signaling in innate immunity.* Science, 1999. **284**(5416): p. 951-5.
36. Zong, D., J. Li, S. Cai, S. He, Q. Liu, J. Jiang, S. Chen, Y. Long, Y. Chen, P. Chen, and R. Ouyang, *Notch1 regulates endothelial apoptosis via the ERK pathway in chronic obstructive pulmonary disease.* Am J Physiol Cell Physiol, 2018. **315**(3): p. C330-C340.
37. Mercer, B.A., N. Kolesnikova, J. Sonett, and J. D'Armiento, *Extracellular regulated kinase/mitogen activated protein kinase is up-regulated in pulmonary emphysema and mediates matrix metalloproteinase-1 induction by cigarette smoke.* J Biol Chem, 2004. **279**(17): p. 17690-6.
38. Yan, G., J. Wang, T. Yi, J. Cheng, H. Guo, Y. He, X. Shui, Z. Wu, S. Huang, and W. Lei, *Baicalin prevents pulmonary arterial remodeling in vivo via the AKT/ERK/NF-κB signaling pathways.* 2019. **9**(4): p. 2045894019878599.

39. Jin, N., N. Hatton, D.R. Swartz, X. Xia, M.A. Harrington, S.H. Larsen, and R.A. Rhoades, *Hypoxia activates jun-N-terminal kinase, extracellular signal-regulated protein kinase, and p38 kinase in pulmonary arteries.* Am J Respir Cell Mol Biol, 2000. **23**(5): p. 593-601.
40. Schermuly, R.T., E. Dony, H.A. Ghofrani, S. Pullamsetti, R. Savai, M. Roth, A. Sydykov, Y.J. Lai, N. Weissmann, W. Seeger, and F. Grimminger, *Reversal of experimental pulmonary hypertension by PDGF inhibition.* J Clin Invest, 2005. **115**(10): p. 2811-21.
41. Kumar, R., C. Mickael, J. Chabon, L. Gebreab, A. Rutebemberwa, A.R. Garcia, D.E. Koyanagi, L. Sanders, A. Gandjeva, M.T. Kearns, L. Barthel, W.J. Janssen, T. Mauad, A. Bandeira, E. Schmidt, R.M. Tuder, and B.B. Graham, *The Causal Role of IL-4 and IL-13 in Schistosoma mansoni Pulmonary Hypertension.* Am J Respir Crit Care Med, 2015. **192**(8): p. 998-1008.
42. Suwanabol, P.A., S.M. Seedial, X. Shi, F. Zhang, D. Yamanouchi, D. Roenneburg, B. Liu, and K.C. Kent, *Transforming growth factor-beta increases vascular smooth muscle cell proliferation through the Smad3 and extracellular signal-regulated kinase mitogen-activated protein kinases pathways.* J Vasc Surg, 2012. **56**(2): p. 446-54.
43. Suwanabol, P.A., S.M. Seedial, F. Zhang, X. Shi, Y. Si, B. Liu, and K.C. Kent, *TGF-beta and Smad3 modulate PI3K/Akt signaling pathway in vascular smooth muscle cells.* Am J Physiol Heart Circ Physiol, 2012. **302**(11): p. H2211-9.
44. Li, L., L. Zhu, B. Hao, W. Gao, Q. Wang, K. Li, M. Wang, M. Huang, Z. Liu, Q. Yang, X. Li, Z. Zhong, W. Huang, G. Xiao, Y. Xu, K. Yao, and Q. Liu, *iNOS-derived nitric oxide promotes glycolysis by inducing pyruvate kinase M2 nuclear translocation in ovarian cancer.* Oncotarget, 2017. **8**(20): p. 33047-33063.
45. Wagner, W., W. Ciszewski, K. Kania, and J. Dastych, *Lactate Stimulates IL-4 and IL-13 Production in Activated HuT-78 T Lymphocytes Through a Process That Involves Monocarboxylate Transporters and Protein Hyperacetylation.* J Interferon Cytokine Res, 2016. **36**(5): p. 317-27.

FIGURE LEGENDS

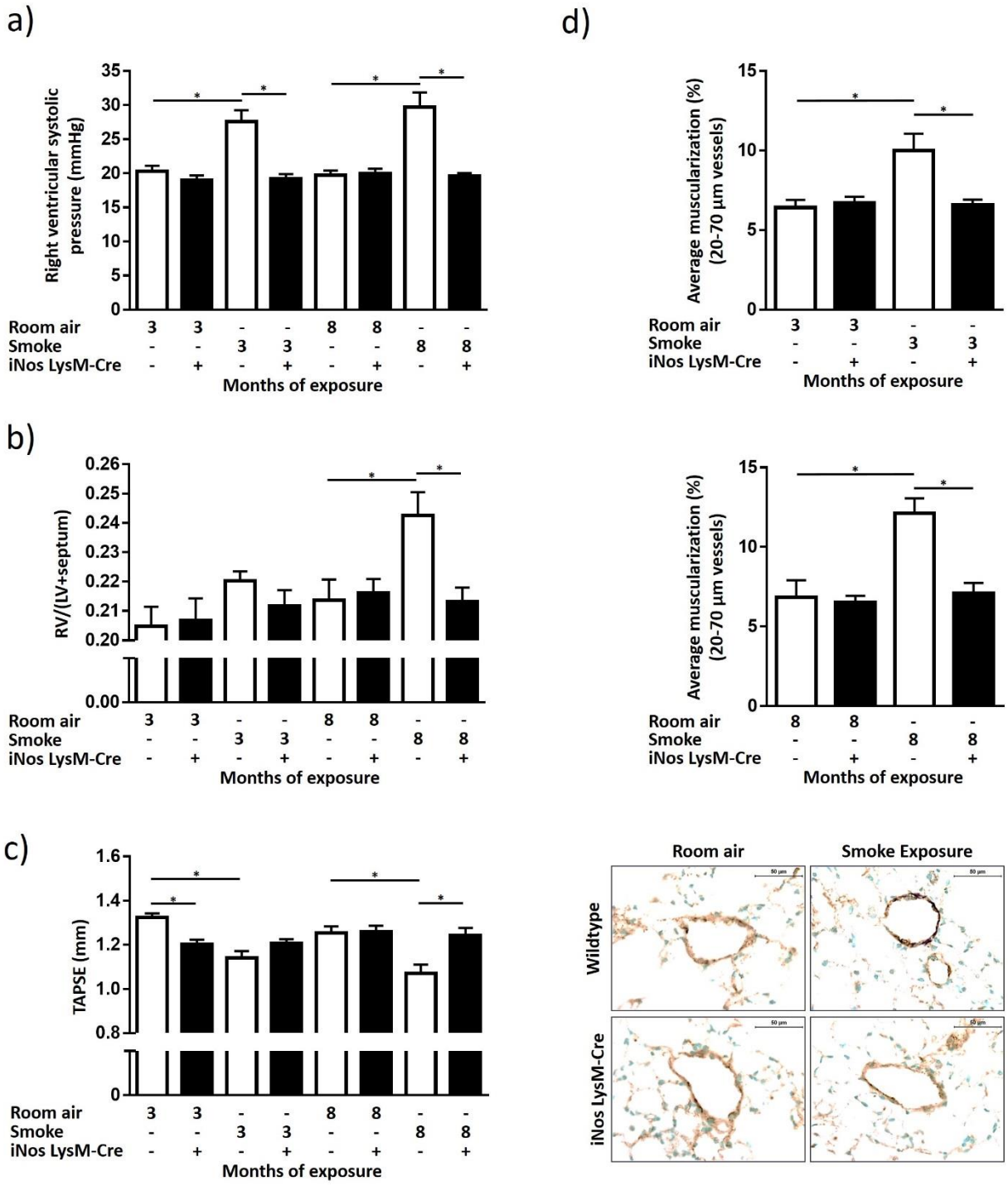

Figure 1:

Myeloid cell type-specific iNOS deletion prevents development of cigarette smoke-induced PH in mice.

Mice were exposed either to cigarette smoke or room air for 3 and 8 months. a) Right ventricular systolic pressure (n=9-12). b) Changes in the right ventricular structure shown as the ratio of the right ventricular (RV) and the left ventricular plus septum (LV+septum) mass (n=9-12). c) Echocardiographic assessment of right ventricular systolic function (n=11-13) depicted by means of tricuspid annular plane systolic excursion (TAPSE). d) Remodelling of the small pulmonary vessels (20-70 µm outer diameter) presented as the average muscularization of total vessel count after 3 (n=4-5, upper) or 8 months of smoke exposure (n=5-7, middle), and representative images of lung sections from mice exposed to cigarette smoke for 8 months and respective room air controls, co-stained against α-smooth muscle actin (purple) and von Willebrand factor (brown). Scale bars = 50 µm. Graphs show mean ± SEM. *$p < 0.05$. Two-way ANOVA (with Tukey´s multiple comparison post-hoc test) was used for statistical analysis.

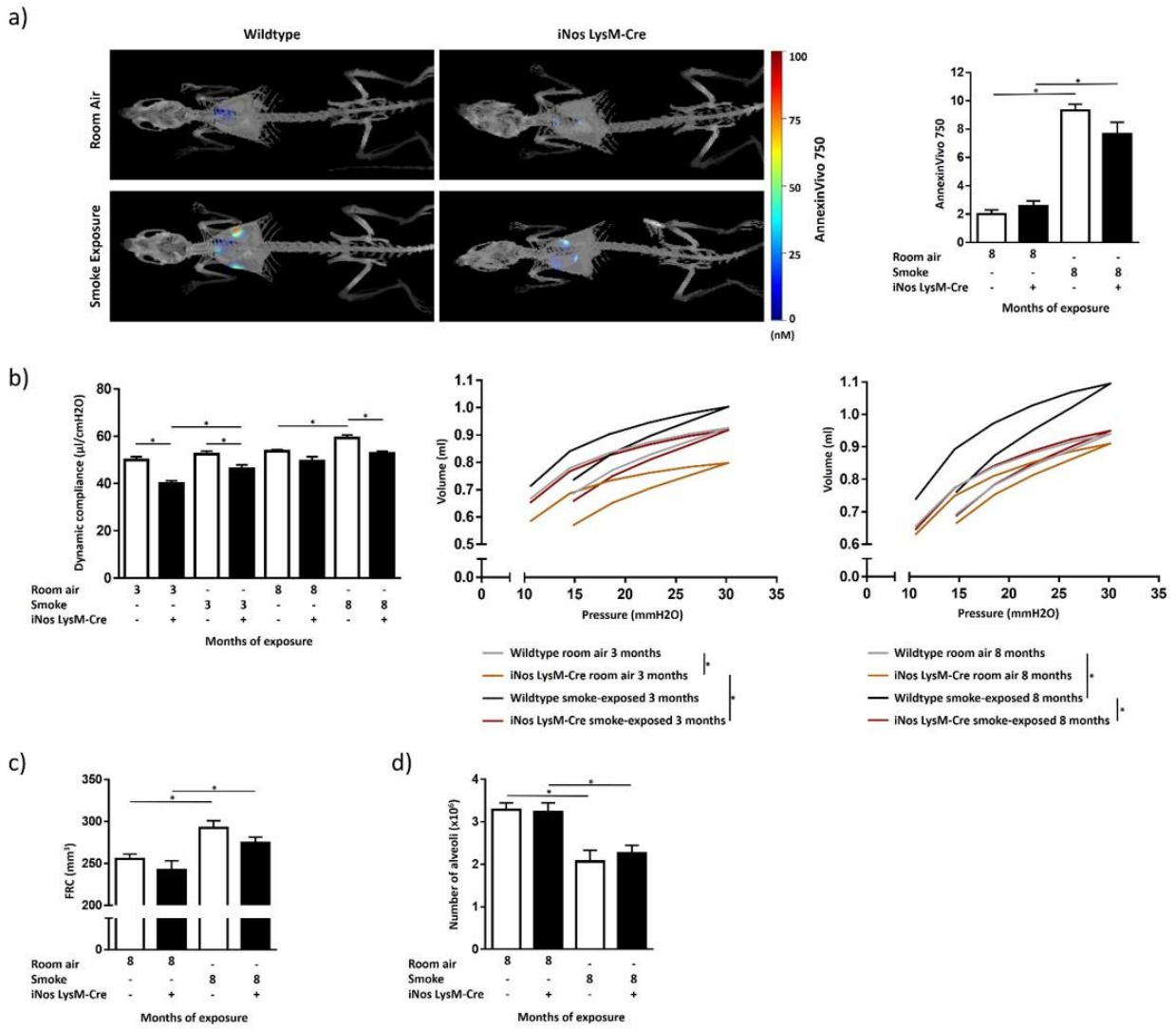

Figure 2:

Chronic smoke exposure leads to emphysema development in myeloid cell type-specific iNOS knockout mice.

Mice were exposed either to cigarette smoke or room air for 3 and 8 months. a) *In vivo* quantification of apoptosis in lungs (n=6-7), detected by a fluorescence molecular tomography (FMT) imaging system, using AnnexinVivo 750 probe. b) Lung function (n=8-11) presented as dynamic compliance (left) and respiratory pressure-volume loops (middle and right). c) Functional residual capacity (FRC) assessed by micro-computed tomography (µCT, n=11-13). d) Number of alveoli (n=7-9) estimated by design-based stereology. Graphs show mean ± SEM. *p

< 0.05. Two-way ANOVA (with Tukey´s multiple comparison post-hoc test) was used for statistical analysis.

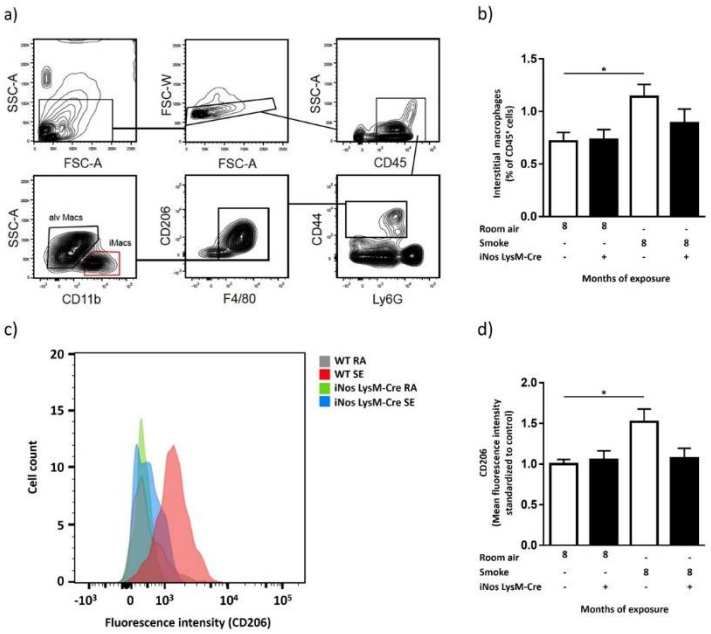

Figure 3:

Myeloid cell-specific iNOS deletion prevents smoke-induced accumulation of interstitial macrophages and upregulation of CD206 (the marker of "M2-like" polarization) on these cells.

Mice were exposed either to smoke (SE) or room air (RA) for 8 months and macrophages in lung homogenates were analysed by flow cytometry. a) Representative flow cytometry gating scheme, used to separate alveolar and interstitial macrophages (SSC – side scatter; FSC – forward scatter). b) Content of interstitial macrophages in the lungs of smoke-exposed mice and respective unexposed (room air) controls (n=4-5), assessed by flow cytometry and given as the percent of $CD45^+$ cells. c) Representative histogram showing $CD206^+$ cells in lungs of wildtype (WT) and myeloid cell-specific iNOS knockout mice. d) CD206 expression on interstitial macrophages (n=4-5), assessed by flow cytometry and given as the mean fluorescence intensity standardized to control. Graphs show mean ± SEM. *$p < 0.05$. Two-way ANOVA (with Tukey´s multiple comparison post-hoc test) was used for statistical analysis.

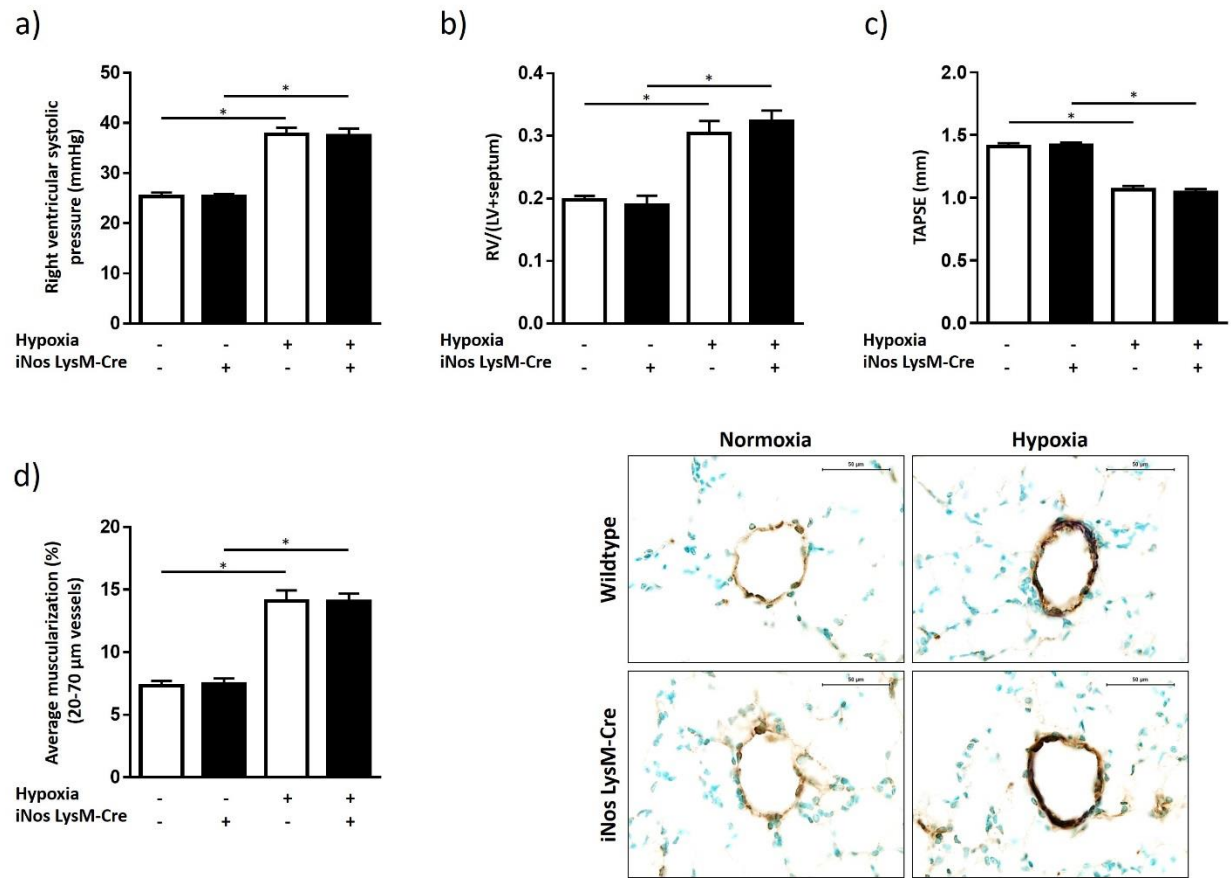

Figure 4:

Myeloid cell-specific iNOS knockout does not protect mice against hypoxia-induced PH.

Mice were exposed to either normobaric normoxia or hypoxia for 28 days. a) Right ventricular systolic pressure (n=6-8). b) Changes in right ventricular structure shown as the ratio of the RV and the left ventricular plus septum (LV+septum) mass (n=6-8). c) Echocardiographic assessment of RV systolic function depicted by means of tricuspid annular plane systolic excursion (TAPSE, n=6-8). d) Remodelling of the small pulmonary vessels (20-70 µm outer diameter) presented as the average muscularization of total vessel count after chronic hypoxia exposure (n=6-8, left), and representative images of lung sections from mice exposed to chronic hypoxia and respective normoxic controls (right), co-stained against α-smooth muscle actin (purple) and von Willebrand factor (brown). Scale bars = 50 µm. Graphs show mean ± SEM. *$p < 0.05$. Two-way ANOVA (with Tukey´s multiple comparison post-hoc test) was used for statistical analysis.

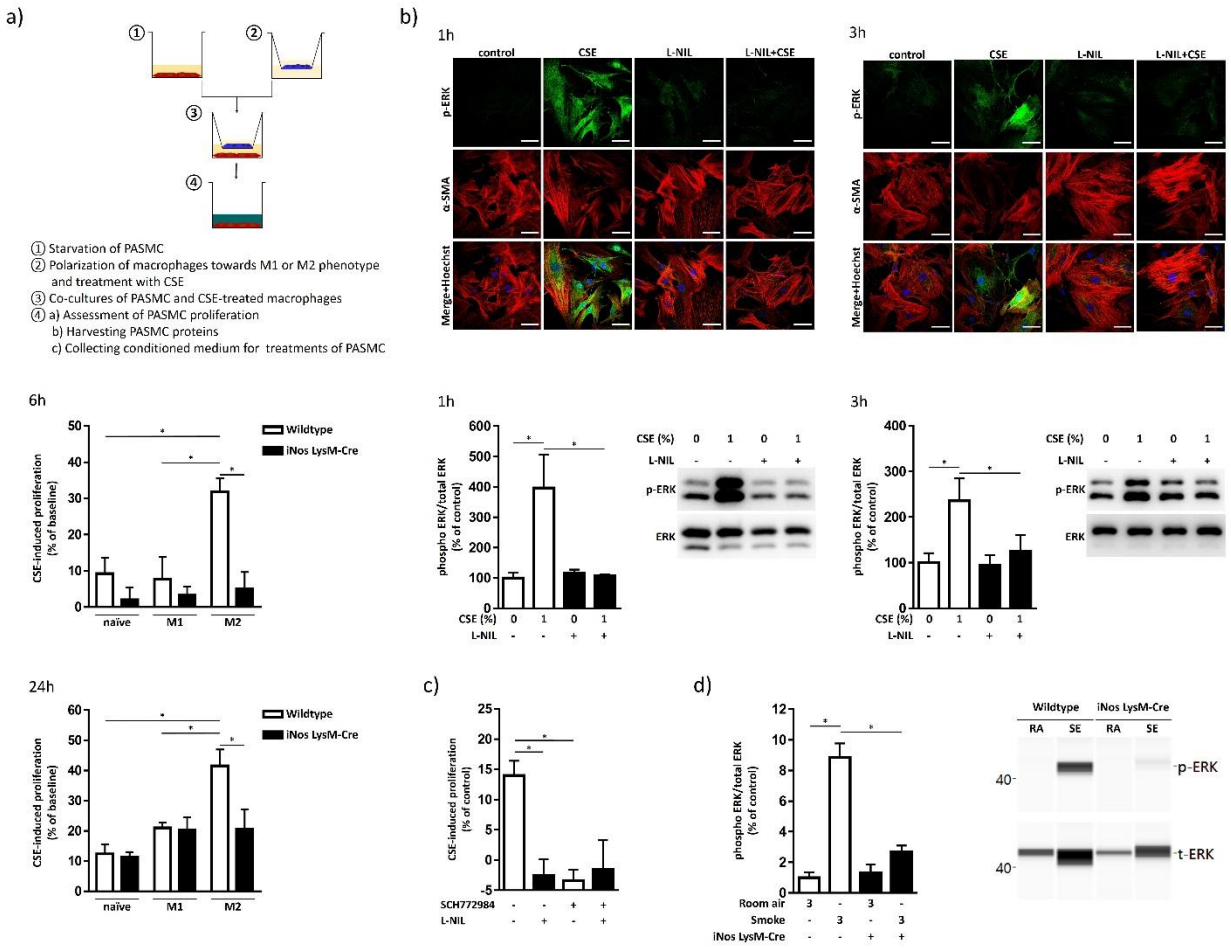

Figure 5:

iNOS activity in macrophages increases proliferation of adjacent PASMC through the activation of the ERK pathway.

PASMC were co-cultured with bone-marrow-derived M0-, M1- or M2-polarized macrophages pre-treated for 3h with 1% cigarette smoke extract (CSE). a) Schematic depiction of the experimental setup for co-culturing bone-marrow-derived macrophages with PASMC (upper panel), and proliferation of PASMC in co-cultures with macrophages assessed by BrdU assay after 6h (n=4, middle panel), and 24h (n=5, lower panel) standardized to control PASMC. Data are given as the difference from the co-culturing with non-CSE exposed controls. b) Representative photos (upper panel) and Western blot analysis (lower panel, n=5) of extracellular signal-regulated kinase (ERK) phosphorylation in PASMC co-cultured with CSE- and/or L-NIL treated M2 cells for

1h and 3h. Data are given as the ratio between phosphorylated and total ERK and standardized to control co-cultures (unexposed to CSE and untreated with L-NIL). PASMC shown in the upper panel are stained for phosphorylated ERK (green), α-smooth muscle actin (α-SMA, red) and counterstained with Hoechst (blue). Scale bars = 50 µm. c) Proliferation of PASMC treated with the ERK inhibitor SCH772984 and conditioned medium (CM) from co-cultures of PASMC and CSE- and/or L-NIL treated M2 macrophages, assessed by BrdU assay. The proliferation is standardized to the control (treatment with PASMC CM). Data are given as the difference between the effects of CM from CSE-exposed and unexposed co-cultures. d) Western blot analysis of the ERK phosphorylation in pulmonary vessels captured by laser microdissection from lungs of animals exposed to smoke for 3 months and respective unexposed controls (n=3). Data are given as the ratio between phosphorylated and total ERK, standardized to control (unexposed WT). Graphs show mean ± SEM. *$p < 0.05$. Two-way ANOVA (with Sidak´s multiple comparison post-hoc test for *in vitro* and Tukey´s multiple comparison post-hoc test for *in vivo* experiments) was used for statistical analysis.

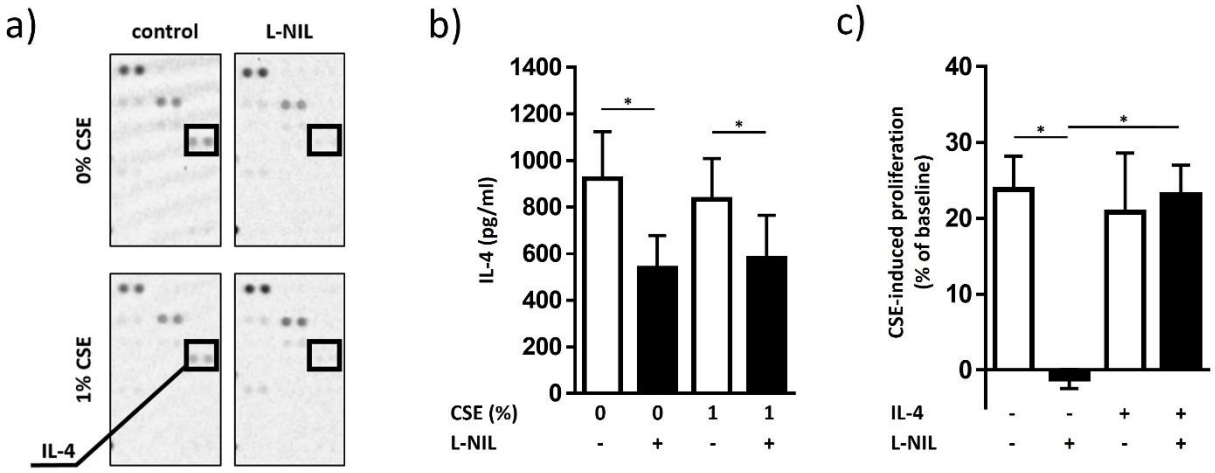

Figure 6:

Interleukin-4 is implicated in CSE-induced pro-proliferative signalling in co-cultures of M2 macrophages and PASMC.

a), b) Interleukin (IL)-4 in the conditioned medium from co-cultures of M2 macrophages with PASMC, assessed by a) cytokine array and b) ELISA assay (n=7). c) CSE-induced proliferation of PASMC in co-cultures with control or L-NIL-treated M2 macrophages, in the absence or presence of IL-4 in the co-culture medium (n=6). Proliferation was assessed by BrdU assay and standardized to the control PASMC. Data are given as the difference from the co-culturing with non-CSE exposed controls. Graphs show mean ±SEM. *$p < 0.05$. Two-way ANOVA (with Sidak´s multiple comparison post-hoc test) was used for statistical analysis.

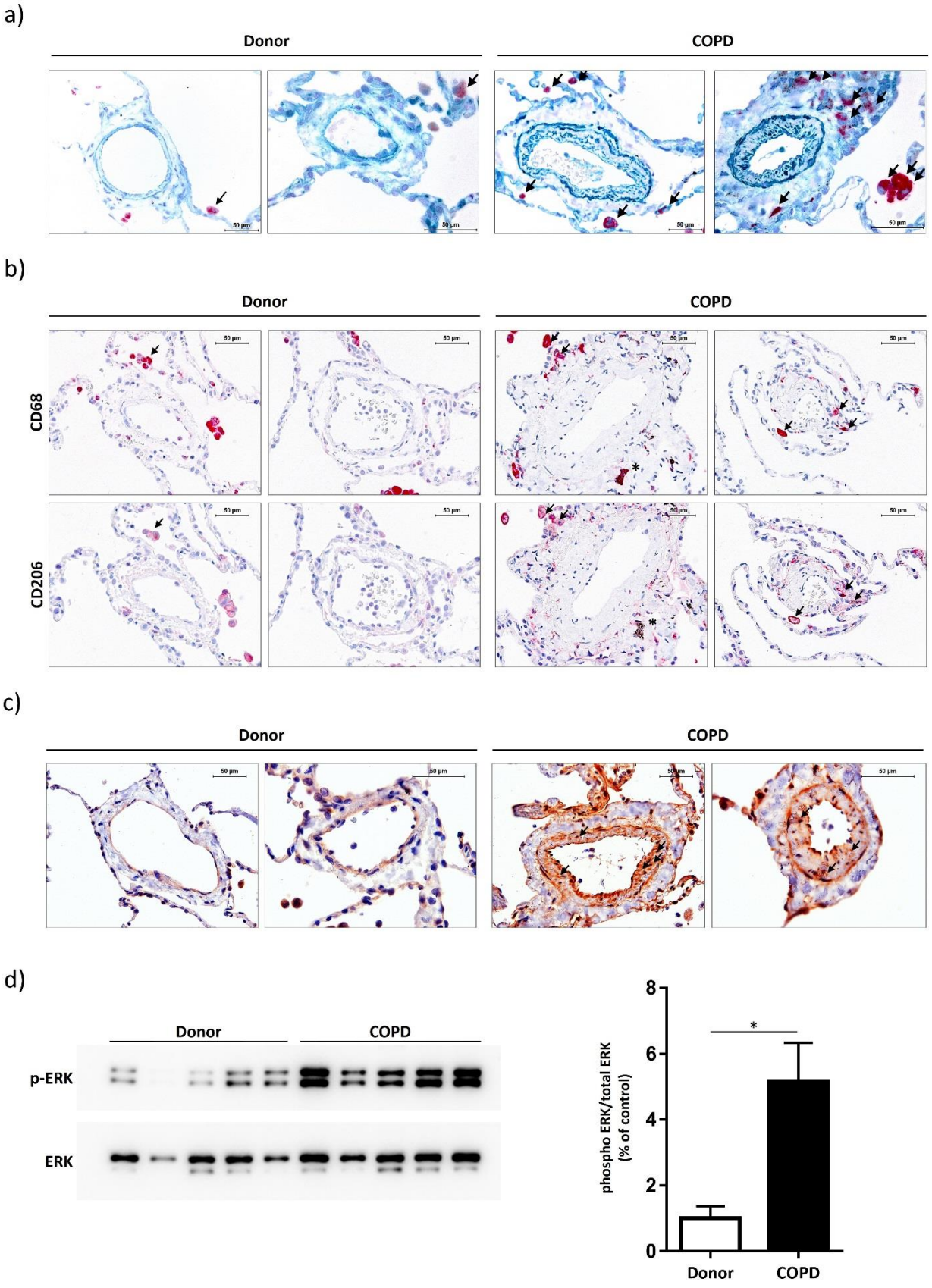
a)
Donor
COPD
b)
Donor
COPD
CD68
CD206
c)
Donor
COPD
d)
Donor
COPD
p-ERK
ERK
phospho ERK/total ERK (% of control)
8
6
4
2
0
*
Donor
COPD

Figure 7:

iNOS$^+$ and CD206$^+$ macrophages accumulate in close proximity of remodelled vessels in lungs from COPD patients.

Representative images of lung sections from donors and COPD patients. a) Co-staining of iNOS (green) and CD68 (red). Arrow: CD68$^+$iNOS$^+$ cells. b) Staining of serial sections for CD68 (red, upper panel) and CD206 (red, lower panel). Arrow: CD68$^+$CD206$^+$ cells. Asterisk: CD68$^+$CD206$^-$ cells. c) Staining for phosphorylated extracellular signal-regulated kinase (ERK, brownish red). Arrow: Positive signal. Scale bars = 50 µm. d) Western blot analysis (n=10 per group) of ERK phosphorylation in lung homogenates of COPD patients and donors. Data are given as the ratio between phosphorylated and total ERK and are standardized to control (donor group). The graph shows mean ± SEM. *$p < 0.05$. A t-test was used for statistical analysis.

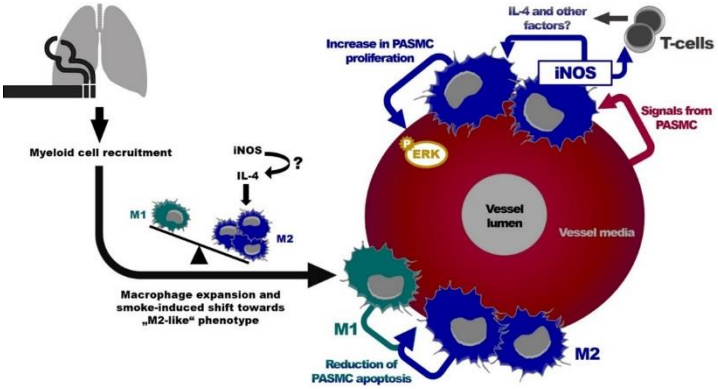

Figure 8:

Scheme of the proposed pathological mechanism underlying smoke-induced vascular remodelling in COPD.

Communication between M2 macrophages and PASMC that leads to extracellular signal-regulated kinase (ERK) activation and PASMC proliferation is potentiated by smoke exposure of macrophages. It depends on iNOS expression in those cells and the IL-4 concentration in the vascular environment.

Myeloid cell-specific deletion of inducible nitric oxide synthase protects against smoke-induced pulmonary hypertension in mice

Marija Gredic, Cheng-Yu Wu, Stefan Hadzic, Oleg Pak, Rajkumar Savai, Baktybek Kojonazarov, Siddartha Doswada, Astrid Weiss, Andreas Weigert, Andreas Guenther, Ralf P. Brandes, Ralph T. Schermuly, Friedrich Grimminger, Werner Seeger, Natascha Sommer, Simone Kraut and Norbert Weissmann

ONLINE SUPPLEMENT

MATERIALS AND METHODS

Experimental design and cigarette smoke exposure

Adult male and female iNos LysM-Cre mice (Nos2$^{tm2904.1Arte}$Tg(CAG-flpe)2ArteLyz2$^{tm1(cre)Ifo}$/), 3-4 months old, and age and gender-matched wildtype (WT) controls (C57BL/6N, obtained from Charles River Laboratories, Sulzfeld, Germany) were randomly allocated to tobacco-smoke-exposed or unexposed group (room air). Thirteen animals per group were subjected to hemodynamic and lung function measurements, echocardiography, fluorescent molecular tomography combined with micro-computed tomography (FMT-µCT) and right heart morphometry. Lungs of animals from each experimental group were randomly allocated to be 1) either paraffin-embedded or cryopreserved or 2) used for either flow cytometry or RNA and protein isolation. N numbers for final analysis vary owing to technical reasons, such as incorrect placement of the catheter or the echocardiographic probe, or to the premature death of some animals. All animal experiments were approved by the regional board for animal welfare (Regierungspräsidium Giessen, Germany).

Mice were exposed to cigarette smoke as described previously [1] and sacrificed after 3 or 8 months.

Chronic hypoxia exposure

Adult male and female Nos2 LysM-Cre mice (Nos2$^{tm2904.1ArteTg}$(CAG-flpe)2ArteLyz2$^{tm1(cre)Ifo}$/), 3-4 months old, and age and gender-matched WT controls (C57BL/6N, obtained from Charles River Laboratories, Sulzfeld, Germany) were exposed to normobaric hypoxia (10% O2) or normobaric normoxia (21% O_2) in a ventilated chamber for 28 days. Experiments were approved by the regional board for animal welfare (Regierungspräsidium Giessen, Germany).

Echocardiography and FMT-µCT

FMT-µCT (FMT; VisEn Medical, Bedford, MA, USA) was performed with Annexin Vivo 750 (Cat# NEV11053; Perkin Elmer, Waltham, USA). Echocardiographic assessment of the right heart structure and function was done one day prior to sacrifice under isoflurane anaesthesia as described previously [2].

Lung function and hemodynamic measurements

For the assessment of lung function, mice were tracheotomized, connected to the FlexiVent mechanical ventilator and data-acquisition system (SCIREQ, Montreal, Canada) and ventilated with a tidal volume of 10ml/kg at a frequency of 150 breaths/min. Snapshot and QuickPrime perturbation were imposed, and pressure-volume loops were generated for assessment of mechanical properties of the respiratory system. Deep inflation was used as a recruitment manoeuvre. Hemodynamic measurements were performed after two to three times repeated lung function measurements, as previously reported [3].

Lung fixation,organ harvest and assessment of right ventricular hypertrophy

Prior to the lung fixation, bronchoalveolar lavage (BAL) was done by introducing and then collecting 700µl of phosphate buffered saline (PBS). This procedure was repeated three times. Then, lung fixation and organ harvesting were done as previously described [4]. After lung fixation, the heart was removed and the weight of the dissected RV and the left ventricle plus septum (LV+S) was deterimined. The Fulton index (RV weight/(LV+S)weight) was calculated as a measure of RV hypertrophy. No significant changes in (LV+S) weight occurred between groups.

Flow cytometry and cell sorting

Single-cell suspensions of cells found either in BAL fluid (BALF) or in the remaining homogenized mouse lung tissue were blocked with FcR blocking reagent (MiltenyiBiotec, Bergisch Gladbach, Germany) in 0.5% PBS-bovine serum albumin (BSA) for 20min, stained with fluorochrome-conjugated antibodies and analyzed on an LSR II/Fortessa flow cytometer or sorted using a FACS Aria III cell sorter (both from BD Biosciences, San Jose, CA, USA). Data were analyzed using FlowJoVx. All antibodies and secondary reagents were titrated to determine optimal concentrations. Comp-Beads (BD Biosciences, San Jose, CA, USA) were used for single-colour compensation to create multicolour compensation matrices. For gating, fluorescence minus one controls were used. The instrument calibration was controlled daily using Cytometer Setup and Tracking beads (BD Biosciences, San Jose, CA, USA). For characterization of lung alveolar and interstitial macrophages (presented in Figure 3) [5, 6], the following antibodies were used: anti-CD11b-BV605, anti-CD44-AlexaFluor700, anti-Ly6G-

APC-Cy7 (BD Biosciences, San Jose, CA, USA), anti-CD45-Vio-Blu (MiltenyiBiotec, Bergisch Gladbach, Germany), anti-CD206 and anti-F4/80-PE-Cy7 (BioLegend, San Diego, CA, USA).

Alveolar and pulmonary vascular morphometry and design-based stereology

Alveolar and pulmonary vascular morphometry, as well as design-based stereology, were performed as previously reported [1] with slight modifications. For the stereological calculations, the volume of the left lung was determined using the buoyancy-based water displacement method [7].

Western Blot analysis

The sample preparation, SDS PAGE electrophoresis, transfer and incubation with primary and secondary antibody were performed as previously described [1], with subtle modifications. Primary antibodies were used as follows: phospho-ERK (p44/p42) (Cat#9101S, Cell Signaling Technology, Danvers, MA, USA) 1:1000; p44/p42 (Cat#9102S, Cell Signaling Technology, Danvers, MA, USA) 1:1000; iNOS (Cat#ab178945, Abcam, Cambridge, UK) 1:1000; β-actin (Cat# b8227, Abcam, Cambridge, UK), 1:20000.

Visualization was done using the Clarity ECL Western Blotting Substrate (Biorad, Hercules, CA, USA) and ChemiDoc Touch Imaging System (Biorad, Hercules, CA, USA).

Laser microdissection and automated Western Blot analysis

Laser microdissection was done as described previously with subtle modifications [8]. Briefly, cryopreserved, Tissue-tek (Sakura Finetek, Staufen, Germany) embedded lung tissue was cut into 12µm thick sections and mounted on membrane-coated glass slides. Sections were stained with haematoxylin (diluted 20:30 with distilled H_2O) for 1min, and dehydrated in the graded ethanol series. 100 vessels per sample were captured by laser microdissection (LMD6000, Leica Microsystems, Wetzlar, Germany) and collected in 30µl of 0.1X Sample buffer (ProteinSimple, San Jose, CA, USA) containing a cOmplete™ Mini EDTA-free Protease-Inhibitor-Cocktail (Roche, Basel, Switzerland). Samples were sonicated (3 times for 30 seconds) and further prepared and analysed using the chemiluminescent detection system of the Jess Simple Western™ platform (ProteinSimple, San Jose, CA, USA) according to the manufacturer´s instructions. Antibodies were used as follows: p-p44/p42 phospho-ERK (p44/p42) (Cat#9101S, Cell Signaling Technology, Danvers, MA, USA) 1:4 and p44/p42 (Cat#9102S, Cell Signaling Technology, Danvers, MA, USA), 1:40.

cDNA synthesis and quantitative PCR (qPCR) analysis

cDNA synthesis and qPCR analysis were done as previously reported [8]. Primer sequences are available upon request.

Isolation of murine pulmonary artery smooth muscle cells (PASMC)

PASMC were isolated from precapillary vessels of 12-16 week old C57BL/6NCrl mice modified from a previously reported protocol [9]. Primary cells were cultured for 5-7 days without passaging in PASMC growth medium (Smooth Muscle Cell Growth Medium 2 (PromoCell, Heidelberg, Germany) + 100µg/ml Normocin (InvivoGen, Vista Sorrento Pkwy San Diego, CA, USA) + 10% (v/v) fetal bovine serum (FBS, Sigma Aldrich, Munich, Germany)). Smooth muscle cells were identified by immunohistochemical staining with smooth muscle cell-specific α-actin and myosin antibodies and examining their morphology. The absence of endothelial cells was confirmed by staining with an antibody directed against von Willebrand factor.

Isolation and differentiation of murine bone marrow-derived macrophages (BMDM)

Tibiae and femora from 12-16 week old C57BL/6NCrl or $Nos2^{tm2904.1Arte}$Tg(CAG-flpe)2ArteLyz2$^{tm1(cre)Ifo}$/ mice were removed under sterile conditions. Isolation of the bone-marrow cells and their differentiation to macrophages was done according to the previously reported protocol [8]. Bone ends were cut off and the bone shafts were then flushed with a 24G needle on a 10ml syringe with PBS without Ca^{2+} and Mg^{2+} (PAN Biotech, Aidenbach, Germany). The harvested bone-marrow was collected in 50ml tubes and centrifuged for 5 min at 400×g at room temperature. Cells were resuspended in BMDM differentiation medium (DMEM/F12 with 10mM L-glutamine, 100IU/ml penicillin, and 100µg/ml streptomycin (all from Gibco, Thermo Fisher Scientific Inc. Waltham, MA, USA), 10% (v/v) FBS (Sigma Aldrich, Munich, Germany) and 35ng/ml recombinant mouse M-CSF (PeproTech, Hamburg, Germany)) and passed through 40µm cell strainer. Cells were counted using a Neubauer hemocytometer and the number was adjusted to $7.5x10^6$ cells/ml. 10ml of cell suspension was seeded per one 10cm non-tissue culture treated Petri dish and cultured in a humidified atmosphere of 5% CO_2 at 37 °C for 7 days, with the addition of 5ml of differentiation medium on day 3. After 7 days, cells were harvested using enzyme-free cell dissociation buffer, seeded at 10^6 cells/ml in the full BMDM culture medium (DMEM/F12 with 10mM L-glutamine, 100IU/ml penicillin, and 100µg/ml streptomycin (all from Gibco, Thermo Fisher Scientific Inc. Waltham, MA, USA) and 10% (v/v) FBS (Sigma Aldrich, Munich, Germany)), and stimulated overnight with 100U/mL

IFN-γ (PeproTech, Hamburg, Germany) to prime them for the differentiation into M1 cells. Next day, IFN-γ was removed and cells were treated with 10ng/ml LPS (Sigma-Aldrich, Munich, Germany) to obtain M1 macrophages, or with 100U/mL IL-4 (PeproTech, Hamburg, Germany) to elicit M2 cells, with or without 100μM L-NIL (Cayman Chemicals, Ann Arbor, MI, USA).

Cigarette smoke extract (CSE) preparation

100% CSE was prepared by vaporizing one 3R4F cigarette (Kentucky Tobacco Research & Development Center, Lexington, USA) within one minute in 10ml of DMEM/F12 (Gibco, Thermo Fisher Scientific Inc. Waltham, MA, USA) medium. Then, it was filtered through a 20μm filter, diluted with the culture medium to the final concentration applied in the experiment and used immediately (in the following 20 minutes) for the cell treatment.

Cell viability assay for CSE-treated macrophages

After 6h of CSE treatment, the new culture medium with 10% (v/v) alamarBlue Cell Viability Reagent (Thermo Fisher Scientific Inc. Waltham, MA, USA) was added. Cell viability was determined after 16h according to the manufacturer's instructions.

Co-cultures of macrophages and PASMC

For experiments with co-cultures of macrophages and PASMC (Figure 5a and 6c), BMDM were seeded at 10^6 cells/mL on Transwell Permeable supports (Corning, New York, NY, USA), differentiated into M1 or M2 cells as described or left in the naïve state. Then, appropriate experimental groups were treated with 1% CSE for 3h. In parallel, PASMC were seeded in 24-well plate dishes at 15.000 cells/well and starved for 24h in PASMC basal medium (PromoCell, Heidelberg, Germany) supplemented with 0.1% FBS. Immediately before co-culturing of these cells, the culture medium was changed for both cell types, and BrdU labelling solution (Roche, Basel, Switzerland) was added to the PASMC. After 6 or 24h, PASMC were fixed and proliferation assay was done according to the manufacturer's instructions. The absorbance of the samples was measured in a microplate reader at 370nm (reference wavelength: 492nm). O.D. value for each experimental sample was standardized to the baseline, i.e. the value measured in control PASMC (that were not co-cultured with macrophages). CSE-dependent proliferation was calculated by subtracting proliferation of CSE-untreated group from the proliferation in corresponding CSE-treated co-cultures.

The experiment focused on the role of IL-4 in the pro-proliferative signalling in co-cultures was done as described, except for 100U/ml of recombinant IL-4 (PeproTech, Hamburg, Germany) added to the co-culture medium of appropriate experimental groups immediately before co-culturing.

E**xperiments with co-culture-conditioned medium (CM)**

For experiments with co-culture CM (Figure 5c, and S5a, b), PASMC and BMDM were co-cultured as previously described. The co-culture CM was collected (after 6h for the experiment shown in Figure 5c, and 24h for the experiment shown in Figures S5b, c), centrifuged for 5 min at 14000×g and kept on -80°C until further use. CM from PASMC monoculture was collected to serve as the control. On the day of the experiment, co-culture CM was thawed and equilibrated to room temperature (RT), and then used as described in the following text for ERK inhibition experiment and for apoptosis and migration assay.

Experiments with Macrophage-CM

For experiments with macrophage conditioned medium (Figure S4b), BMDM were seeded at 10^6 cells/mL in 24-well plates and left overnight in a humidified atmosphere of 5% CO_2 at 37 °C. Macrophages were differentiated into M1 or M2 cells as described. After the treatment with 1% CSE for 3h, the medium was changed and macrophages were cultured for the additional 24h, after which period CM was collected.

PASMC were seeded in 24-well plate dishes at 15.000 cells/well and starved for 24h in PASMC basal medium (PromoCell, Heidelberg, Germany) supplemented with 0.1% FBS. Then, the medium was replaced by the fresh medium containing 1) BrdU labelling solution (Roche, Basel, Switzerland) and 2) 50% CM collected from macrophage monocultures as described. After 24h, proliferation was measured according to the manufacturer's instructions and the O.D. values were standardized to the appropriate baseline (PASMC treated with fresh BMDM medium instead of macrophage-CM).

ERK inhibition experiment

PASMC were seeded in 96-well plate dishes at 5000 cells/well and starved for 24h in PASMC basal medium (PromoCell, Heidelberg, Germany) supplemented with 0.1% FBS. Cells were pre-treated with DMSO or 100µM SCH772984 for 3h. Afterwards, the medium was replaced by a fresh medium containing 1) BrdU labelling solution (Roche, Basel, Switzerland), 2) either

DMSO (solvent) or 100µM SCH772984 (Selleckchem, Houston, TX, USA) in DMSO, and 3) 50% of either co-culture CM (collected after 6h co-culturing) or control CM from PASMC monocultures. After 24h, proliferation was measured according to the manufacturer's instructions. Values were standardized to the appropriate baseline (either DMSO+PASMC CM-treated cells or SCH772984 inhibitor+PASMC CM-treated cells). CSE-dependent proliferation was calculated by subtracting the proliferation in the group treated with CM from CSE-unexposed co-cultures from the proliferation in the corresponding group treated with CM from CSE-exposed co-cultures (e.g. M2 CSE CM-M2 CM; or M2 L-NIL CSE CM-M2 L-NIL CM).

Apoptosis assay

PASMC were seeded at a density of 5000 cells/well in 96 well plates. Apoptosis kinetic assay (Abcam, Cambridge, UK) was done according to the manufacturer's instruction and IncuCyte ZOOM (Essen BioScience, Ann Arbor, MI, USA) was used for visualization. CSE, previously reported to induce apoptosis of murine primary PASMC [8], was used as a pro-apoptotic signal.

Migration assay

PASMC were seeded in 24 well plates containing 2 Well Culture-Inserts (Ibidi, Fitchburg, WI, USA) at 18000 cells/well and left overnight (5% CO_2, 37°C). The next day, inserts were removed, cells were washed twice with PBS and treated with 50% of co-culture CM or control macrophage growth medium. Closure of the wound made by insert's removal was followed using IncuCyte ZOOM for 24h and results are given as the percentage of wound confluence.

Cytokine array and ELISA assays

CM from co-cultures was harvested after 24h, centrifuged and kept at -80°C. On the day of the experiment, 400µl of CM was thawed on ice and assayed using Proteome Profiler Mouse XL Cytokine Array (R&D Systems, Minneapolis, MN, USA) according to the manufacturer's instructions. ELISA assay for IL-4 (R&D Systems, Minneapolis, MN, USA), was done in duplicates and following manufacturer's instructions, with 50µl of CM (pre-thawed and equilibrated to the RT) per well.

Immunocytochemical staining of PASMC

Murine PASMC were seeded on collagen-coated glass coverslips and co-cultured with M2 macrophages as previously described. At the respective time-points, cells were pre-fixed with 2% paraformaldehyde (PFA) added in co-culturing medium for 5 minutes, and then fixed with 4% PFA for additional 15 minutes at RT. After washing with PBS, cells were permeabilized with ice-cold 100% methanol for 10 minutes at -20°C and rinsed with PBS. Blocking was done for 1h at RT using 5% BSA 0.3% TritonX in PBS, and slides were incubated overnight at 4°C with a phospho-p44/p42 antibody (Cat#4370, Cell Signaling Technology, Danvers, MA, USA, 1:200) diluted in 1% BSA 0.3% TritonX in PBS. Following day, slides were washed with PBS and incubated with a Cy3-labelled α-smooth muscle actin antibody (Cat#C6198, Sigma-Aldrich, Munich, Germany 1:400) and Alexa488-labelled goat anti-rabbit secondary antibody (Cat#A-11034, Thermo Fisher Scientific Inc. Waltham, MA, USA, 1:400) for 2h at RT. After washing in PBS, cells were counterstained with 2µg/ml Hoechst in PBS for 10 min. Slides were mounted using Fluoro Care Anti-Fade Mountant (Biocare Medical) and analysed by confocal microscopy. At least three images from randomly chosen fields were taken for analysis.

Immunofluorescent staining of murine lungs

For immunofluorescent staining of mouse lung sections for CD68 and iNOS, 3µm thick serial sections of paraffin-embedded lung tissue were deparaffinised, rehydrated and antigen retrieval was done using Rodent Decloaker (Biocare Medical, Pacheco, CA, USA). Non-specific antibody binding was avoided by incubation of sections in 10% BSA for 1 h and in Background Punisher (Biocare Medical, Pacheco, CA, USA) for 15 minutes at RT. Following overnight incubation with both primary antibodies for iNOS (Cat#3523, Abcam, Cambridge, UK, 1:50) and CD68 (Cat#NB100-683, Novus Biologicals, Littleton, CO, USA, 1:50) at 4°C, slides were washed 3 times with PBS pH 7.4 and incubated with fluorescently labelled secondary antibodies (Cat#A-11034 and A-21422, Thermo Fisher Scientific Inc. Waltham, MA, USA, 1:400) for 2h at RT. After washing in PBS, sections were counterstained with DAPI and mounted using Fluoro Care Anti-Fade Mountant (Biocare Medical, Pacheco, CA, USA).

SUPPLEMENTARY DISCUSSION

Distinctiveness of smoke-induced inflammatory milieu driving pulmonary vascular remodelling in COPD

Alveolar hypoxia resulting from the impairment of respiratory function has long since been considered the main cause of the pulmonary vascular remodelling seen in COPD patients. Identification of M2 macrophages, which were previously implicated in the development of hypoxic PH [10-12] as a critical cell type driving smoke-induced pulmonary vascular remodelling may suggest that this pathological event is driven by similar, hypoxia-dependent mechanisms. However, myeloid cell type-specific iNOS knockout animals developed hypoxia-induced PH and RV hypertrophy similar to wild-type mice. Given the phenotypical plasticity of macrophages and the spectrum of activation states that these cells are able to acquire, it is not surprising that specific pathways can be activated and are preferentially involved in (pathological) signalling events underlying vascular remodelling, depending on external stimuli and the microenvironmental milieu such as the one present in cigarette-smoke exposed lungs. Additionally, our result is in line with the recent hypothesis that pulmonary vascular remodelling is an early pathological event in COPD that occurs prior to the alveolar destruction and resulting hypoxemia. In this regard, we previously showed that 8 months of tobacco-smoke exposure in mice did not lead to hypoxemia [1]. The proposed sequence of vascular remodelling and alveolar destruction is substantiated by evidence from animal models [1, 8, 13-15] and human tissues [16, 17]. Going deeper into the matter our study provides further substantial evidence for the existence of smoke-specific signalling events underlying the remodelling of the pulmonary vasculature, independent from alveolar destruction. Our findings, if transferable to the human situation, can have an impact on the development of new treatment strategies for COPD-PH.

iNOS as a modulator of inflammatory cell phenotype and composition in smoke-induced PH

The second important consequence of myeloid cell-specific iNOS deletion on the composition of inflammatory cell infiltrates is the preserved proportion of T-cells in the population of lung immune cells, as opposed to the situation in smoke-exposed WT mice, where the portion of T-cells in lung inflammatory infiltrates is increased. Although assessment of absolute numbers is difficult due to smoke-induced dynamic changes of most cell populations in lungs, this

finding suggests that lungs of smoke-exposed knockout mice have decreased T-cell numbers. This is of interest as an increased number of T-cells has been implicated in other forms of PH [18-20] and found in perivascular inflammatory infiltrates of COPD patients [16, 21]. Macrophage derived-iNOS could influence endothelial activation and T-cell diapedesis, as described for the T-cell extravasation into tumours [22]. Alternatively, changes in T-cell populations might be the consequence of the still largely undeciphered impact of macrophage-derived iNOS on T-cell differentiation and activity. However, as Lysozyme M also labels a small portion of T- and B-cells, a more specific mouse line will be valuable for the further investigation of this phenomenon [23].

Factors influencing the assessment of cell proliferation in a co-culture setup

Analysing results from our numerous experiments done using the same co-culturing protocol, we observed differences in the response of PASMC to the same stimulus (in this case, co-culturing with CSE-exposed M2 macrophages) between experiments. These differences can be explained by the fact that assessment of proliferation was done using a BrdU assay, a technique semi-quantitative in nature. Moreover, in such setups, slight variations can occur due to 1) small differences during the above-described isolation of mouse primary PASMC and BMDM, or 2) variations introduced during seeding of the cells. 3) The need for the synchronized growth of two different primary cell types can further aggravate possible subtle discrepancies. 4) The respective experiments were done several years apart and 5) small batch-to-batch differences in products such as FBS, IL-4 or M-CSF could also account for the observed changes. A varying amplitude of changes in proliferation measured by BrdU in similar experimental conditions is, however, in accordance with the literature [24-28].

LITERATURE

1. Seimetz, M., N. Parajuli, A. Pichl, F. Veit, G. Kwapiszewska, F.C. Weisel, K. Milger, B. Egemnazarov, A. Turowska, B. Fuchs, S. Nikam, M. Roth, A. Sydykov, T. Medebach, W. Klepetko, P. Jaksch, R. Dumitrascu, H. Garn, R. Voswinckel, S. Kostin, W. Seeger, R.T. Schermuly, F. Grimminger, H.A. Ghofrani, and N. Weissmann, *Inducible NOS inhibition reverses tobacco-smoke-induced emphysema and pulmonary hypertension in mice.* Cell, 2011. **147**(2): p. 293-305.
2. Kojonazarov, B., S. Hadzic, H.A. Ghofrani, F. Grimminger, W. Seeger, N. Weissmann, and R.T. Schermuly, *Severe Emphysema in the SU5416/Hypoxia Rat Model of Pulmonary Hypertension.* Am J Respir Crit Care Med, 2019. **200**(4): p. 515-518.
3. Pradhan, K., A. Sydykov, X. Tian, A. Mamazhakypov, B. Neupane, H. Luitel, N. Weissmann, W. Seeger, F. Grimminger, A. Kretschmer, J.P. Stasch, H.A. Ghofrani, and R.T. Schermuly, *Soluble guanylate cyclase stimulator riociguat and phosphodiesterase 5 inhibitor sildenafil ameliorate pulmonary hypertension due to left heart disease in mice.* Int J Cardiol, 2016. **216**: p. 85-91.
4. Hadzic, S., C.Y. Wu, M. Gredic, B. Kojonazarov, O. Pak, S. Kraut, N. Sommer, D. Kosanovic, F. Grimminger, R.T. Schermuly, W. Seeger, S. Bellusci, and N. Weissmann, *The effect of long-term doxycycline treatment in a mouse model of cigarette smoke-induced emphysema and pulmonary hypertension.* Am J Physiol Lung Cell Mol Physiol, 2021.
5. Schyns, J., F. Bureau, and T. Marichal, *Lung Interstitial Macrophages: Past, Present, and Future.* J Immunol Res, 2018. **2018**: p. 5160794.
6. Misharin, A.V., L. Morales-Nebreda, G.M. Mutlu, G.R. Budinger, and H. Perlman, *Flow cytometric analysis of macrophages and dendritic cell subsets in the mouse lung.* Am J Respir Cell Mol Biol, 2013. **49**(4): p. 503-10.
7. Scherle, W., *A simple method for volumetry of organs in quantitative stereology.* Mikroskopie, 1970. **26**(1): p. 57-60.
8. Seimetz, M., N. Sommer, M. Bednorz, O. Pak, C. Veith, S. Hadzic, M. Gredic, N. Parajuli, B. Kojonazarov, S. Kraut, J. Wilhelm, F. Knoepp, I. Henneke, A. Pichl, Z.I. Kanbagli, S. Scheibe, A. Fysikopoulos, C.Y. Wu, W. Klepetko, P. Jaksch, C. Eichstaedt, E. Grunig, K. Hinderhofer, M. Geiszt, N. Muller, F. Rezende, G. Buchmann, I. Wittig, M. Hecker, A. Hecker, W. Padberg, P. Dorfmuller, S. Gattenlohner, C.F. Vogelmeier, A. Gunther, S. Karnati, E. Baumgart-Vogt, R.T. Schermuly, H.A. Ghofrani, W. Seeger, K. Schroder, F. Grimminger, R.P. Brandes, and N. Weissmann, *NADPH oxidase subunit NOXO1 is a target for emphysema treatment in COPD.* Nat Metab, 2020. **2**(6): p. 532-546.
9. Marshall, C., A.J. Mamary, A.J. Verhoeven, and B.E. Marshall, *Pulmonary artery NADPH-oxidase is activated in hypoxic pulmonary vasoconstriction.* Am J Respir Cell Mol Biol, 1996. **15**(5): p. 633-44.
10. Abid, S., E. Marcos, A. Parpaleix, V. Amsellem, M. Breau, A. Houssaini, N. Vienney, M. Lefevre, G. Derumeaux, S. Evans, C. Hubeau, M. Delcroix, R. Quarck, S. Adnot, and L. Lipskaia, *CCR2/CCR5-mediated macrophage-smooth muscle cell crosstalk in pulmonary hypertension.* Eur Respir J, 2019. **54**(4).
11. Vergadi, E., M.S. Chang, C. Lee, O.D. Liang, X. Liu, A. Fernandez-Gonzalez, S.A. Mitsialis, and S. Kourembanas, *Early macrophage recruitment and alternative activation are critical for the later development of hypoxia-induced pulmonary hypertension.* Circulation, 2011. **123**(18): p. 1986-95.

12. Amsellem, V., S. Abid, L. Poupel, A. Parpaleix, M. Rodero, G. Gary-Bobo, M. Latiri, J.L. Dubois-Rande, L. Lipskaia, C. Combadiere, and S. Adnot, *Roles for the CX3CL1/CX3CR1 and CCL2/CCR2 Chemokine Systems in Hypoxic Pulmonary Hypertension.* Am J Respir Cell Mol Biol, 2017. **56**(5): p. 597-608.
13. Wright, J.L. and A. Churg, *Effect of long-term cigarette smoke exposure on pulmonary vascular structure and function in the guinea pig.* Exp Lung Res, 1991. **17**(6): p. 997-1009.
14. Ferrer, E., V.I. Peinado, M. Diez, J.L. Carrasco, M.M. Musri, A. Martinez, R. Rodriguez-Roisin, and J.A. Barbera, *Effects of cigarette smoke on endothelial function of pulmonary arteries in the guinea pig.* Respir Res, 2009. **10**: p. 76.
15. Wright, J.L., T. Ngai, and A. Churg, *Effect of long-term exposure to cigarette smoke on the small airways of the guinea pig.* Exp Lung Res, 1992. **18**(1): p. 105-14.
16. Peinado, V.I., J.A. Barbera, P. Abate, J. Ramirez, J. Roca, S. Santos, and R. Rodriguez-Roisin, *Inflammatory reaction in pulmonary muscular arteries of patients with mild chronic obstructive pulmonary disease.* Am J Respir Crit Care Med, 1999. **159**(5 Pt 1): p. 1605-11.
17. Santos, S., V.I. Peinado, J. Ramirez, T. Melgosa, J. Roca, R. Rodriguez-Roisin, and J.A. Barbera, *Characterization of pulmonary vascular remodelling in smokers and patients with mild COPD.* Eur Respir J, 2002. **19**(4): p. 632-8.
18. Pullamsetti, S.S., R. Savai, W. Janssen, B.K. Dahal, W. Seeger, F. Grimminger, H.A. Ghofrani, N. Weissmann, and R.T. Schermuly, *Inflammation, immunological reaction and role of infection in pulmonary hypertension.* Clin Microbiol Infect, 2011. **17**(1): p. 7-14.
19. Bonnet, S., G. Rochefort, G. Sutendra, S.L. Archer, A. Haromy, L. Webster, K. Hashimoto, S.N. Bonnet, and E.D. Michelakis, *The nuclear factor of activated T cells in pulmonary arterial hypertension can be therapeutically targeted.* Proc Natl Acad Sci U S A, 2007. **104**(27): p. 11418-23.
20. Tuder, R.M., B. Groves, D.B. Badesch, and N.F. Voelkel, *Exuberant endothelial cell growth and elements of inflammation are present in plexiform lesions of pulmonary hypertension.* Am J Pathol, 1994. **144**(2): p. 275-85.
21. SAETTA, M., S. BARALDO, L. CORBINO, G. TURATO, F. BRACCIONI, F. REA, G. CAVALLESCO, G. TROPEANO, C.E. MAPP, P. MAESTRELLI, A. CIACCIA, and L.M. FABBRI, *CD8 + ve Cells in the Lungs of Smokers with Chronic Obstructive Pulmonary Disease.* 1999. **160**(2): p. 711-717.
22. Sektioglu, I.M., R. Carretero, N. Bender, C. Bogdan, N. Garbi, V. Umansky, L. Umansky, K. Urban, M. von Knebel-Doberitz, V. Somasundaram, D. Wink, P. Beckhove, and G.J. Hammerling, *Macrophage-derived nitric oxide initiates T-cell diapedesis and tumor rejection.* Oncoimmunology, 2016. **5**(10): p. e1204506.
23. Ye, M., H. Iwasaki, C.V. Laiosa, M. Stadtfeld, H. Xie, S. Heck, B. Clausen, K. Akashi, and T. Graf, *Hematopoietic stem cells expressing the myeloid lysozyme gene retain long-term, multilineage repopulation potential.* Immunity, 2003. **19**(5): p. 689-99.
24. Liu, G., P. Hao, J. Xu, L. Wang, Y. Wang, R. Han, M. Ying, S. Sui, J. Liu, and X. Li, *Upregulation of microRNA-17-5p contributes to hypoxia-induced proliferation in human pulmonary artery smooth muscle cells through modulation of p21 and PTEN.* Respir Res, 2018. **19**(1): p. 200.
25. Kim, F.Y., E.A. Barnes, L. Ying, C. Chen, L. Lee, C.M. Alvira, and D.N. Cornfield, *Pulmonary artery smooth muscle cell endothelin-1 expression modulates the*

pulmonary vascular response to chronic hypoxia. Am J Physiol Lung Cell Mol Physiol, 2015. **308**(4): p. L368-77.

26. Shan, R., L. Chen, X. Li, H. Wu, Q. Liang, and X. Tang, *Hypoxia promotes rabbit pulmonary artery smooth muscle cells proliferation through a 15-LOX-2 product 15(S)-hydroxyeicosatetraenoic acid.* Prostaglandins Leukot Essent Fatty Acids, 2012. **86**(1-2): p. 85-90.
27. Das, M., N. Burns, S.J. Wilson, W.M. Zawada, and K.R. Stenmark, *Hypoxia exposure induces the emergence of fibroblasts lacking replication repressor signals of PKCzeta in the pulmonary artery adventitia.* Cardiovasc Res, 2008. **78**(3): p. 440-8.
28. Ten Freyhaus, H., E.M. Berghausen, W. Janssen, M. Leuchs, M. Zierden, K. Murmann, A. Klinke, M. Vantler, E. Caglayan, T. Kramer, S. Baldus, R.T. Schermuly, M.D. Tallquist, and S. Rosenkranz, *Genetic Ablation of PDGF-Dependent Signaling Pathways Abolishes Vascular Remodeling and Experimental Pulmonary Hypertension.* Arterioscler Thromb Vasc Biol, 2015. **35**(5): p. 1236-45.

FIGURE LEGENDS

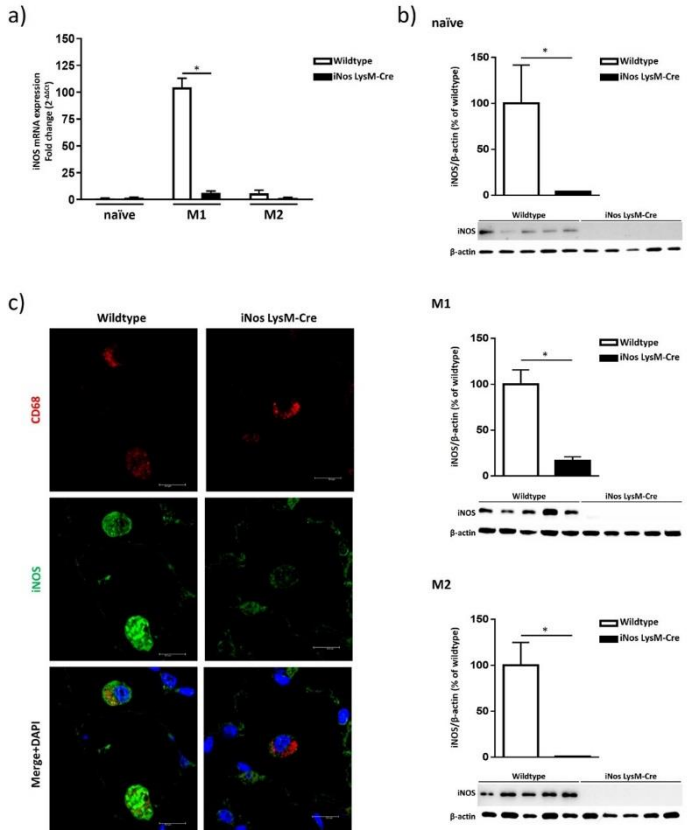

Figure S1: *iNos* gene deletion in myeloid cells using iNos LysM-Cre driver line.

Bone-marrow-derived macrophages were isolated from wildtype (WT) and iNos LysM-Cre mice and polarized *in vitro* using either interferon (IFN)-γ and lipopolysaccharide (LPS) to elicit M1 polarization, or interleukin (IL)-4 to achieve an M2 phenotype. a) Expression of *iNos* gene in naïve, M1 and M2 macrophages, quantified by real-time PCR. Graph shows mean ± SEM. *p < 0.05. Two-way ANOVA (with Sidak´s multiple comparison post-hoc test) was used. b) Western blot quantification of iNOS protein levels in naïve (upper), M1 (middle) and M2 (lower panel) macrophages. Graphs show mean ± SEM. *p < 0.05. Unpaired t-test was used for statistical analysis. c) Representative images of lung sections from WT and iNos LysM-Cre mice stained for CD68 (red) and iNOS (green) and counterstained with DAPI (blue). Scale bar = 10 µm.

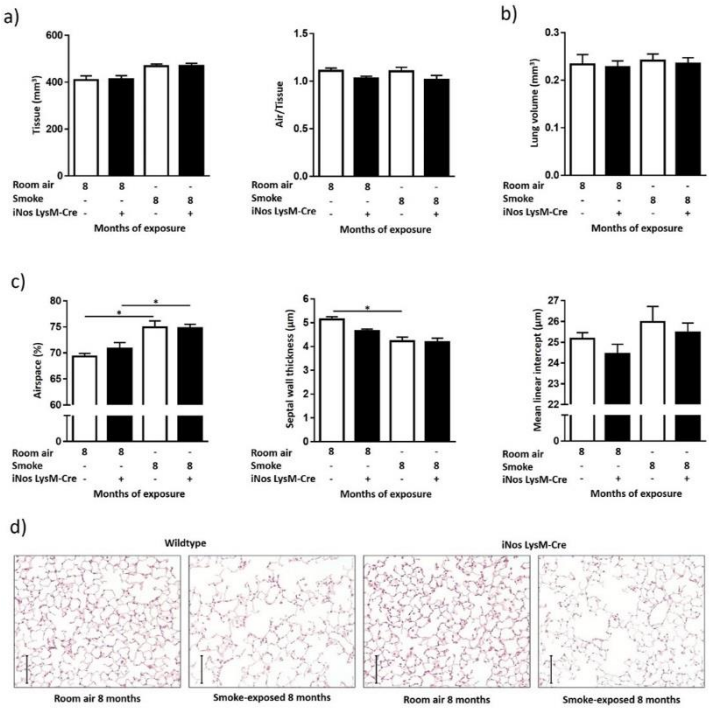

Figure S2: Analysis of lung structure after chronic smoke exposure

Wildtype and myeloid cell-specific iNOS knockout mice were exposed to smoke for 8 months. a) Tissue volume (left) and air/tissue ratio (right) in lungs of mice exposed to smoke for 8 months and respective unexposed (room air) controls (n=11-13), based on micro-computed tomography (µCT) imaging. b) Lung volume in mice after 8 months of smoke exposure, assessed by the water displacement method (n=7-9). c) Alveolar morphometry (n=6-7) showing the percentage of airspace (left), septal wall thickness (middle) and mean linear intercept (right) in mice after 8 months of smoke exposure. Graphs show mean ± SEM. *p < 0.05. Two-way ANOVA (with Tukey´s multiple comparison post-hoc test) was used. d) Representative images of lung sections from mice after 8 months of smoke exposure stained with haematoxylin-eosin (H&E). Scale bar = 100 µm.

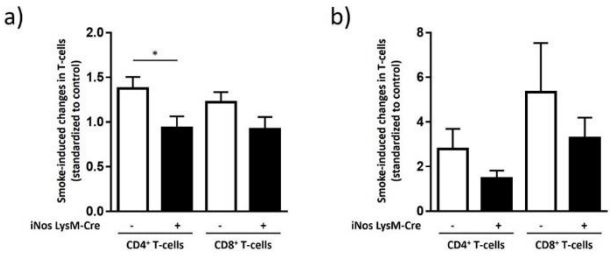

Figure S3: Flow cytometry analysis of T-cells in broncho-alveolar lavage fluid and lung homogenate of mice after 8 months of smoke exposure

a) $CD4^+$ T-lymphocytes and $CD8^+$ T-lymphocytes in lung homogenate. b) $CD4^+$ T-lymphocytes and $CD8^+$ T-lymphocytes found in the BALF (n=4-5). All values are given as the percentage of $CD45^+$ cells standardized to non-exposed control. Graphs show mean ± SEM. *$p < 0.05$. Statistical analysis was done by unpaired T-test.

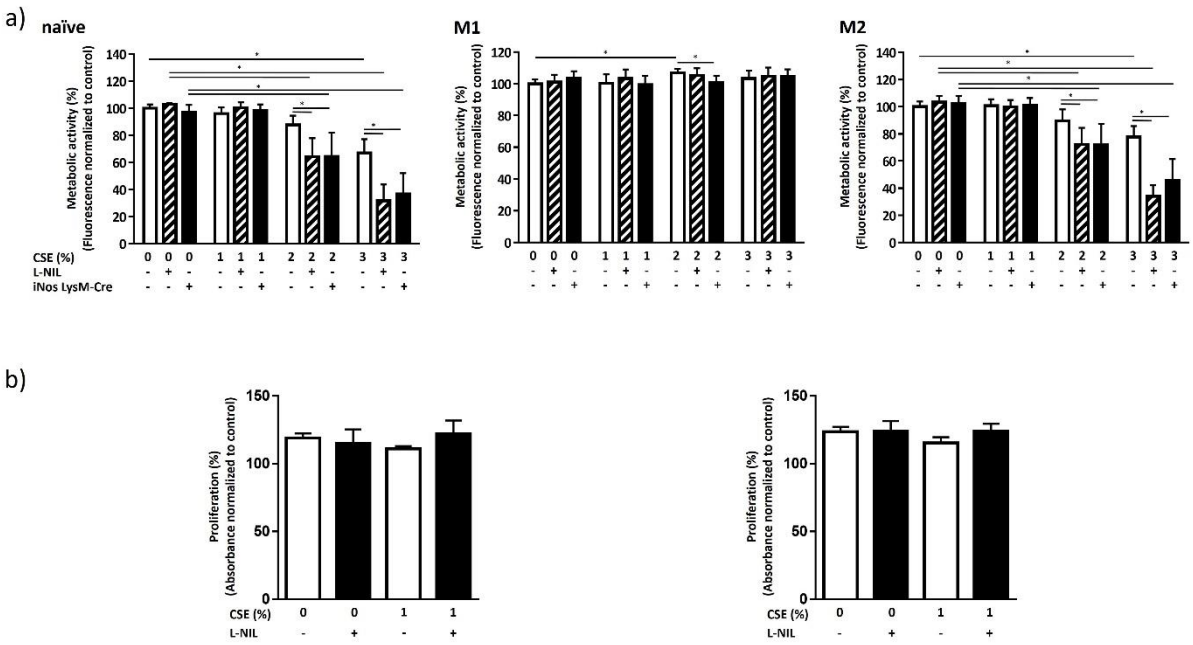

Figure S4: Analysis of smoke-induced changes in monocultures of bone marrow-derived macrophages

a) Metabolic activity of control, iNOS-deficient and L-NIL-treated M0, M1 and M2 macrophages after exposure to cigarette smoke extract (CSE), measured by alamarBlue assay and given as the percentage of control (n=6). b) Proliferation of mouse pulmonary artery smooth muscle cells (PASMC) during 24h of incubation with culture-conditioned medium from M1- (left) or M2- (right) polarized macrophages pre-treated with CSE, measured by BrdU incorporation assay and given as the percentage of control (n=4). Graphs show mean ± SEM. *p < 0.05. Two-way ANOVA (with Sidak´s multiple comparison post-hoc test) was used for statistical analysis.

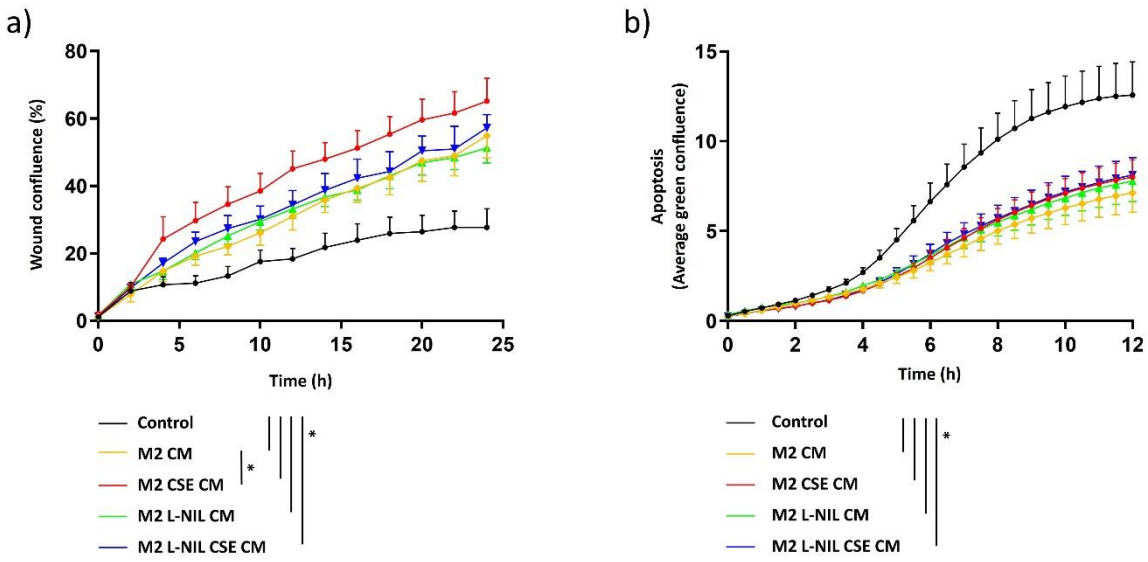

Figure S5: Investigation of the effect of the crosstalk between macrophages and PASMC on migration and apoptosis of PASMC

a) Migration of PASMC treated with conditioned medium (CM) from co-cultures of PASMC and control or CSE and/or L-NIL-treated M2 macrophages (n=5). Data are given as the percentage of wound confluence. b) Apoptosis of PASMC treated with CM from co-cultures of PASMC and control or CSE and/or L-NIL-treated M2 macrophages (n=5), given as the confluence of cells labelled with annexin. Graphs show mean ± SEM. *p < 0.05. Two-way ANOVA (with Sidak´s multiple comparison post-hoc test) was used for statistical analysis.

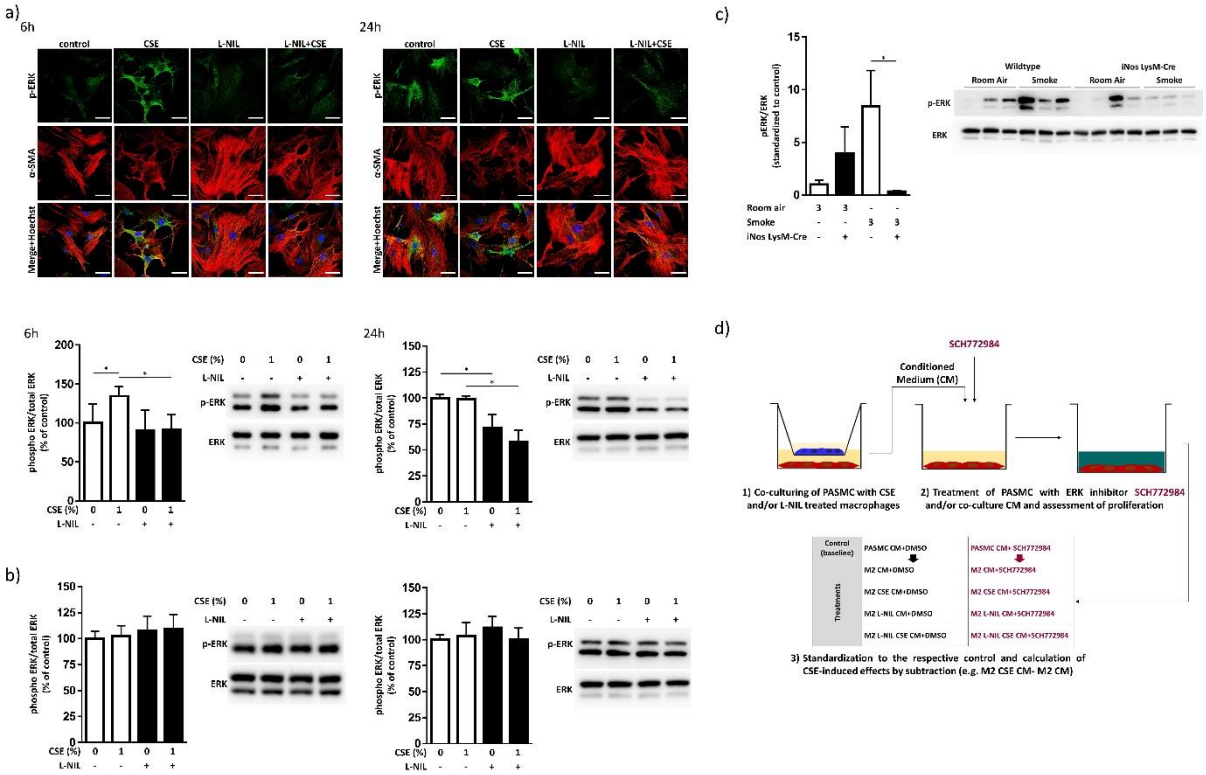

Figure S6: Investigation of the ERK pathway activation in co-cultured PASMC and mouse lung homogenates

a) Representative photos (upper panel) and Western blot analysis (lower panel) of ERK phosphorylation in PASMC co-cultured with CSE- and/or L-NIL treated M2 cells for 6h and 24h. Data are given as the ratio between phosphorylated and total ERK and standardized to control co-cultures (unexposed to CSE and untreated with L-NIL, n=4-5). PASMC shown on the upper panel are stained for phosphorylated extracellular signal-regulated kinase (ERK, green), α-smooth muscle actin (α-SMA, red) and counterstained with Hoechst (blue). Scale bars = 50 µm. b) Western blot analysis of ERK phosphorylation in PASMC co-cultured with M0 (left) and M1 (right) macrophages for 24h (n=4). Data are given as the ratio between phosphorylated and total ERK and standardized to control co-cultures (unexposed to CSE and untreated with L-NIL). c) Western blot analysis of the ERK phosphorylation in lung homogenates from animals exposed to smoke for 3 months and respective unexposed controls (n=6-7). Data are given as the ratio between phosphorylated and total ERK, standardized to control (unexposed WT mice). d) Schematic representation of the experimental design for assessing the effects of the extracellular signal-regulated kinase (ERK) inhibitor on the CSE-induced pro-proliferative signalling in co-cultures. Graphs show mean ± SEM. *$p < 0.05$. Two-way ANOVA (with Sidak´s

multiple comparison post-hoc test for *in vitro* and Tukey´s multiple comparison post-hoc test for *in vivo* experiments) was used for statistical analysis.